The Pennsylvania State University

The Graduate School

Department of Chemical Engineering

EFFECTS OF HEMODYNAMIC FORCES ON ENDOTHELIAL CELL HYDRAULIC CONDUCTIVITY

A Thesis in

Chemical Engineering

by

Zhengyu Pang

Submitted in Partial Fulfillment
of the Requirements
for the Degree of

Doctor of Philosophy

August 2003

The thesis of Zhengyu Pang has been reviewed and approved* by the following:

John M. Tarbell
Distinguished Professor of Chemical Engineering and Bioengineering
Thesis Adviser
Chair of Committee

James S. Ultman
Distinguished Professor of Chemical Engineering and Bioengineering

Abdellaziz Ben-Jebria
Professor of Chemical Engineering and Bioengineering

Norman R. Harris
Associate Professor of Bioengineering

Henry Foley
Professor of Chemical Engineering
Head and Walter L. Robb Family Endowed Chair of the
Department of Chemical Engineering

* Signatures are on file in the Graduate School.

ABSTRACT

Starling's hypothesis that fluid movement across the microvascular wall is determined by the transmural differences in hydrostatic and osmotic pressures was tested using an *in vitro* model comprised of bovine aortic endothelial cells (BAECs) grown on a porous support. In all experiments a 1% bovine serum albumin (BSA) solution was maintained in the abluminal reservoir and the luminal reservoir contained either a 1% or a 5.5% BSA solution. The global osmotic pressure difference across the endothelial layers was thus either 0 or 20.3 cm H_2O. When the luminal concentration of BSA was changed from 1% to 5.5% at a hydrostatic pressure differential of 5, 10 or 20 cm H_2O, no reverse flow (in the reabsorption direction) was observed even though the hydrostatic pressure differential was far below the global osmotic pressure differential. In another case, the hydrostatic pressure differential was dropped quickly from 20 to 5 cm H_2O while a constant osmotic pressure differential was maintained by 5.5% BSA in the luminal reservoir. A strong transient reabsoption flow was observed over a 30 second period which diminished to undetectable levels within 2.5 minutes; then a sustained steady state filtration flow was observed after 20 minutes. These *in vitro* experiments support other studies in capillaries showing transient reabsorption that decays to steady state filtration at longer times.

Human umbilical vein endothelial cells (HUVECs) and BAECs display opposite hydraulic conductivity (L_P) responses to shear stress. In HUVECs, 5, 10, and 20 dyne/cm^2 steady shear stress transiently increased L_P of endothelial cells (ECs), and L_P returned to normal after a two hour exposure to shear stress. Pure oscillatory shear stress

of 0 ± 20 dyne/cm^2 had no effect in changing L_P. Furthermore, superposition of oscillatory shear stress on steady shear stress suppressed the effect induced by steady shear stress. Shear reversal was not necessary for the oscillatory shear stress to function. This phenomenon is very different from BAEC which showed a significant sustained increase in L_P for steady shear stress and only oscillatory shear stress with shear reversal could exert an inhibitory effect on steady shear stress induced increase in L_P.

Intracellular calcium was first investigated for its role in the signal transduction pathway between shear and L_P. The addition of BAPTA-AM (10 uM), an intracellular calcium chelator, reduced the baseline L_P by 40% over a period of 10 minutes, significantly different from 20% due to the "sealing effect" over the same period, suggesting the involvement of a calcium pathway in the regulation of hydraulic conductivity. The transient increase in L_P of HUVEC in response to 1 U/ml thrombin, that is known to be calcium dependent, was delayed by incubation with 10 uM BAPTA-AM for 30 minutes, confirming the requirement of calcium in the thrombin response. However, the transient increase of L_P by shear stress does not seem to be calcium dependent, because blocking of intracellular calcium pathway by using BATPA-AM had no effect in blocking the shear response of L_P.

Shear stress also increased nitric oxide (NO) production in HUVEC. However, the shear response of HUVEC L_P did not seem to be NO dependent. Increasing NO concentration with SNAP (500 uM), an exogenous NO donor, had no effect on HUVEC L_P, while decreasing of NO production with L-NMMA (100 uM), a nitric oxide

synthase (NOS) inhibitor, had no effect on shear response of HUVEC L_P. Other pathways than calcium and NO must be involved in the shear response.

Finally the total content and phosphorylation state of the tight junction protein occludin was investigated under experimental conditions. 1 U/ml thrombin and 10 dyne/cm^2 shear stress increased occludin phosphorylation significantly at time 30 minutes, which was consistent with the time profile of L_P in response to thrombin and shear, respectively. 10 ± 15 dye/cm^2 oscillatory shear stress, 500 uM SNAP, and 100 uM L-NMMA did not change occludin phosphorylation while they had no effect on L_P as compared with controls, suggesting that occludin phosphorylation is a determining factor for hydraulic conductivity. The total amount of occludin did not change after the application of steady and oscillatory shear stresses, but 1 U/ml thrombin decreased occludin total content at 30 minutes, suggesting that phosphorylation of occludin led to occludin degradation and L_P elevation.

TABLE OF CONTENTS

LIST OF FIGURES

LIST OF TABLES

ACKNOWLEDGEMENTS

I would like to thank my mentor and thesis advisor, Dr. John M. Tarbell who provided me with an extraordinary amount of patience, encouragement, and enthusiasm during the development of this study. His insightful observation and ability to pull the essence from messy experiments will have a longtime impact on me. I would also like to thank my committee members Dr. James Ultman, Dr. Abdellaziz Ben-Jebria, and Dr. Norman Harris for their time and invaluable assistance. Special thanks go to my colleague, and now Ph.D. graduate, Lucas DeMaio, who provided me with free service to collect human umbilical cords and shipped them promptly to my lab.

I wish to thank Dr. Mechteld Hillsley and Sunitha Lakshminarayanan for their training in cell culture, John Artman and Mike Dancu, who wrote the nice data acquisition programs for Jv, Dr. David Antonetti for his assistance in Western blotting, Dr. Perdue for his sharing of expertise and for generous use of his laboratory facilities. I would also like to thank to my other labmates: Dr. Yuchen Qiu, Mete Civelek, Dr. Su Wang, Jeff Garanich, Danielle Berardi, Kristy Ainslie, Andrew Fitting, Jason Kosky for the great time we spent together. I also want to thank Elaine and Susan from Center for Quantitative Cell Analysis for their technical assistance for the confocal microscopy and flow cytometry.

Finally and most significantly, I would like to give my whole-hearted thanks to my wife, Jie , for the time we went through together and for her assistance with Matlab, and Mathematica. I also want to thank to my parents, Jun Pang and Yinfen Lu, who always encouraged me to pursue the work I like and to be a benefit for the society.

This work was supported by NHLBI/NIH Grant R01 HL 57093.

Chapter 1

Introduction

Hemodynamics plays an important role in the normal function of endothelial cells. The circulation system supplies nutrients and oxygen from the blood to the interstitium to maintain homeostasis. This process is precisely and efficiently regulated by the endothelial cells, which separate the blood from the interstitium. It is expected that shear stress (flow) increases the permeability of endothelial cells. When high demands of nutrients are needed, an increase in flow rate takes place. For materials whose transport is limited by the endothelium, their endothelial permeability needs to be increased accordingly. Several *in vivo* studies provide evidence that endothelial permeability is indeed sensitive to alterations of fluid shear stress. Lever *et al.* [1]observed that hydraulic conductivity of rabbit carotid arteries in an *ex vivo* flow loop increased significantly after 20 minutes of exposure to shear stress of 1 dyne/cm^2 on the vessel wall. Yuan observed a 48% increase in albumin permeability when the intraluminal perfusion velocity was increased from 7 to 13 mm/s [2]. Finally, Shibata and Kamiya, using rabbit tenuissimus muscle, reported an increase in permeability of Cr-EDTA (m.w. 341) as flow was elevated [3].

Hemodynamics is also believed to play a role in atherosclerosis, as evidenced by the distribution of atherosclerotic lesions. Regions of low and oscillatory shear stress [4, 5], such as branches and sharp curvatures, have a great predilection for the localization of

the disease, where the transport rate of low-density lipoprotein increases [6]. In this case, however, low and oscillatory shear stress is related to high permeability.

Therefore, shear stress acts differently on endothelial permeability under different scenarios. To make things more complicated, the effect of shear stress on endothelial permeability differs spatially in the circulation network. Williams' experiments on frog mesentery reported that shear stress increased venular capillary hydraulic conductivity while it had little effect on arteriolar capillary hydraulic conductivity [7].

Sill *et al*. [8], using the *in vitro* model developed in our lab demonstrated that endothelial monolayer hydraulic conductivity was elevated by shear stress. However, Chang *et al*. [9] showed that shear stress failed to increase hydraulic conductivity in cultured HUVECs. HUVECs, by nomenclature, are classified as venous EC. Structurally and functionally, however, they are more like arterial cells. In the fetal circulation, the umbilical vein carries oxygenated blood and is surrounded by a thick layer of smooth muscle cells, thus having the structure of a large, muscular artery. The strikingly different responses to shear stress exhibited by these two cell lines are of great interest in this study. The comparison of these two cell lines will shed light on understanding the different mechanisms of shear stress responses, which might be general in physiology.

In this study, a comparison study between HUVECs and BAECs was conducted with the emphasis on HUVECs. The volume flux (Jv/A) of HUVECs in response to various shear stresses (steady and oscillatory) was obtained using a well-established *in vitro* model in our lab, followed by the study of the shear stress regulation mechanism, which was carried out at two levels: the signal transduction pathway level (including intracellular calcium pathway and NO pathway) using agonists and antagonists, and the

protein level (total content of occludin and phosphorylation states of occludin) using Western blotting and Protein DC method.

In this study, we also investigated Starling's hypothesis using cultured BAEC monolayers (sections 2.2, 3.11.1~ 3.11.3, 4.1, and 5.1) for the further validation of our *in vitro* model. Recent *in vivo* studies by Michel [10]and Weinbaum [11]suggested that the driving forces in Starling's hypothesis were not determined by the global concentrations in the blood and the interstitium, but by the local pericapillary concentrations. Therefore, fluid reabsorption by way of Starling's mechanism was demonstrable in short term experiments, but not on a long-term steady state basis. We conducted experiments paralleling those described by Michel and Phillips [10], to test whether the modified Starling's hypothesis was also demonstrable in our *in vitro* model.

Chapter 2

Background

2.1 Shear Stress and Endothelial Cells

Blood vessels are composed of three layers: intima, media, and adventitia. Endothelial cells (ECs) line the intima, the innermost part of the blood vessel, and are believed to play an important role in homeostasis. ECs continuously experience three forces imparted by flowing blood: normal pressure, circumferential stress induced by the pressure, and axial tangential shear stress.

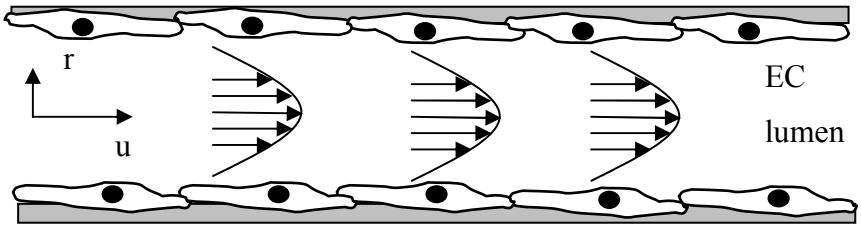

Figure **2-1**: Blood vessel and endothelial cells

Shear stress (τ) is defined as:

$$\tau = -\mu \frac{du}{dr} \qquad \textbf{2.1}$$

where $\frac{du}{dr}$ is the velocity gradient in the radial direction and μ is the viscosity of the blood (Figure **2-1**). Shear stress (dyne/cm^2) acts as an indicator of flow rate. Endothelial cells sense the change of the blood flow through the shear stress acting on their surface.

Barrier function is usually measured by transendothelial electrical resistance (TER), hydraulic conductivity (L_P) and solute permeability (*Pe*). Water, albumin, and LDL, representing different sizes of molecules, are very suitable subjects for studying EC transport properties. This research focuses on hydraulic conductivity of endothelial cells.

2.2 Driving Force for the Hydraulic Conductivity

Starling's pioneering hypothesis that fluid movement across microvascular walls is determined by the transmural difference in hydrostatic and oncotic pressures [12]has become a general principle of cardiovascular and renal physiology[13]. Starling noted that higher protein concentration in the plasma acts as an opposing force to the hydrostatic pressure and that hydrostatic and oncotic pressures reach a balance which determines the flux. The Starling relationship between the transmural fluid flow rate per unit area of capillary wall, Jv/A, and the differentials between capillary and interstitial values of hydrostatic pressure, $P_c - P_i$, and osmotic pressure, $\pi_c - \pi_i$, is usually expressed as

$$Jv/A = L_P \cdot [P_c - P_i - \sigma \cdot (\pi_c - \pi_i)] \qquad \textbf{2.2}$$

where L_P, the hydraulic conductivity, and σ, the reflection coefficient, are properties of the capillary wall. An inference of the classical Starling hypothesis is that there is a net filtration in the capillaries on the arterial side and readsorption (flow against the hydrostatic pressure gradient) on the venous side where the osmotic pressure differential is higher than hydrostatic pressure differential.

Studies by Intaglietta and Zwiefach [14]challenged the notion that significant reabsorption occurs at the venous end of the microcirculation where the osmotic force exceeds the hydrostatic force. Their investigations indicated that fluid reabsorption by way of the Starling mechanism was demonstrable in short term experiments (where protein does not attain steady-state distribution in the extravascular space), but not on a long-term, steady state basis. This was clearly confirmed by Michel and Phillips[10] who performed experiments on isolated, perfused, frog mesenteric microvessels using the Landis technique and observed transient reabsorption over a period of 15-30 seconds after the hydrostatic pressure was dropped below the osmotic pressure, as expected from Starling's law. When the measurements were extended 2 to 5 minutes after the pressure drop, however, there was no evidence of reabsorption even though the osmotic pressure was significantly greater than the hydrostatic pressure.

To explain this paradox in the steady state, Michel and Phillips [10]presented a novel assumption that the pericapillary concentration, C_i, that determines π_i in Eq. **2.2** was given by a mixing condition such that

$$C_i = Js / Jv \qquad \textbf{2.3}$$

where Js is transmural flow rate of the osmotic solute. In general, C_i differs from the global tissue concentration, which in experiments is typically fixed by bathing solutions or external reservoirs. This assumption, when combined with the classical convective coupling equation for solute transport [15], leads to the following modified Starling law .

$$\frac{Jv}{A} = L_P(P_c - P_i) - L_P\sigma^2\pi_c \frac{1-\exp(-Pe)}{1-\sigma\exp(-Pe)} \qquad \textbf{2.4}$$

where

$$Pe = Jv(1-\sigma)/P_d \qquad \textbf{2.5}$$

is the Peclet number and P_d is the diffusive permeability of albumin. This theory predicts that when the solute permeability is finite, steady state reabsorption of fluid from tissue to capillary cannot be maintained by the Starling mechanism alone.

A much more detailed microstructural model of the endothelial transport barrier accounting for the surface glycocalyx layer and the fine structure of the inter-endothelial tight junction has provided further insight into the Starling mechanism [11, 16]. This model predicts that the Starling forces are determined by the local differences in hydrostatic and osmotic pressures across the surface glycocalyx layer. Additional experiments in frog mesenteric microvessels which support this new view of Starling's hypothesis have been reported recently [16].

The controlled experiments which support a modified Starling hypothesis have been limited to frog mesenteric capillaries. Our group, and many others, have studied endothelial transport properties using *in vitro* models comprised of cultured endothelial cells grown on porous supports [9, 17, 18]. To further test the Starling hypothesis, in the present study we used an *in vitro* model which was well established in our laboratory,

bovine aortic endothelial cells (BAECs) on polycarbonate filters, and conducted experiments paralleling those described by Michel and Phillips[10] and Hu *et al*.[16]. We also observed transient reabsorption after lowering hydrostatic pressure which reverted to filtration in the steady state.

2.3 Molecular Architecture and Regulation of Endothelial Barrier Function

Most molecules pass through the endothelium by one of two mechanisms: paracellular pathway or transcelluar pathway. For water and small hydrophilic molecules (radius < 3 nm), transport is primarily through clefts between neighboring cells. Therefore, small solute permeability is correlated with hydraulic conductivity, which is in large part regulated by cell junctions localized in cell clefts and by the cytoskeleton. For the large molecules, such as LDL, vesicular transport (transcellular pathway) is believed to play a more important role[19].

2.3.1 The cytoskeleton

Cell shape change induced by the cytoskeleton affects the physical dimensions of the clefts as well as the structures of cell junctions, indicating a fundamental role of the cytoskeleton in regulating EC permeability. The cytoskeleton is composed of three types of protein filaments—actin filaments, microtubules, and intermediate filaments. Among them, actin filaments are the most important for cell shape regulation, which can be achieved through active contraction and passive retraction. Actin, along with myosin,

adenosine 5'-triphosphate (ATP), and Ca^{2+}/ calmodulin, forms the contractile system in ECs . Myosin is composed of myosin light chain (MLC) and myosin heavy chain with the former determining the activity of myosin. Myosin's sliding along actin filaments (F-actin) leads to cell contraction. This myosin-actin complex is termed stress fiber or actomyosin. In contrast to the activation of cell contractility, passive retraction of cells can occur independently of myosin light chain kinase (MLCK). This process may be regulated by phosphorylation of linking proteins such as vinculin and talin that link cell junction proteins at cell-cell contacts and by transmembrane integrins at cell-matrix contacts to the cytoskeleton [20].

Actomyosin interaction controls the paracellular pathway of vascular permeability and is mediated by phosphorylation of MLC by myosin light chain kinase (MLCK) or Rho kinase or dephosphorylation of MLC by MLC phosphatase [21, 22]. Several lines of evidence underscore the essential role of the cytoskeleton in EC permeability regulation. Upon exposure to shear stress, actin filaments rearrange to create bundles of stress fibers, drawing the peripheral regions away from bordering cells. The round endothelial cells elongate and line up with the direction of flow (shear stress)[23]. Pretreatment of endothelial cells with 7-nitrobenz-2-oxa-1,3-diazole (NBD)-phallicidin (an actin-stabilizing agent) prevented the thrombin-induced cell shape change as well as the increase in transendothelial permeability, indicating that the shift in actin filament distribution in response to permeability-increasing mediators is a major factor in the loss of the endothelial barrier [24].

2.3.2 Tight junctions, adherens junctions and gap junctions

Three types of junctions, namely, gap junctions, tight junctions and adherens junction, have been discovered in ECs [25, 26] (Figure **2-2)**. Gap junctions are clusters of transmembrane hydrophilic channels that allow for direct exchange of ions and small molecules between adjacent cells. Therefore, they are usually not considered vital in the transport of molecules from the blood to the interstitium. The role of adherens junctions in the regulation of permeability has been recently discovered [27, 28] , and is not covered in this study. Tight junctions play a crucial role in permeability modulation, and become a focus in this study.

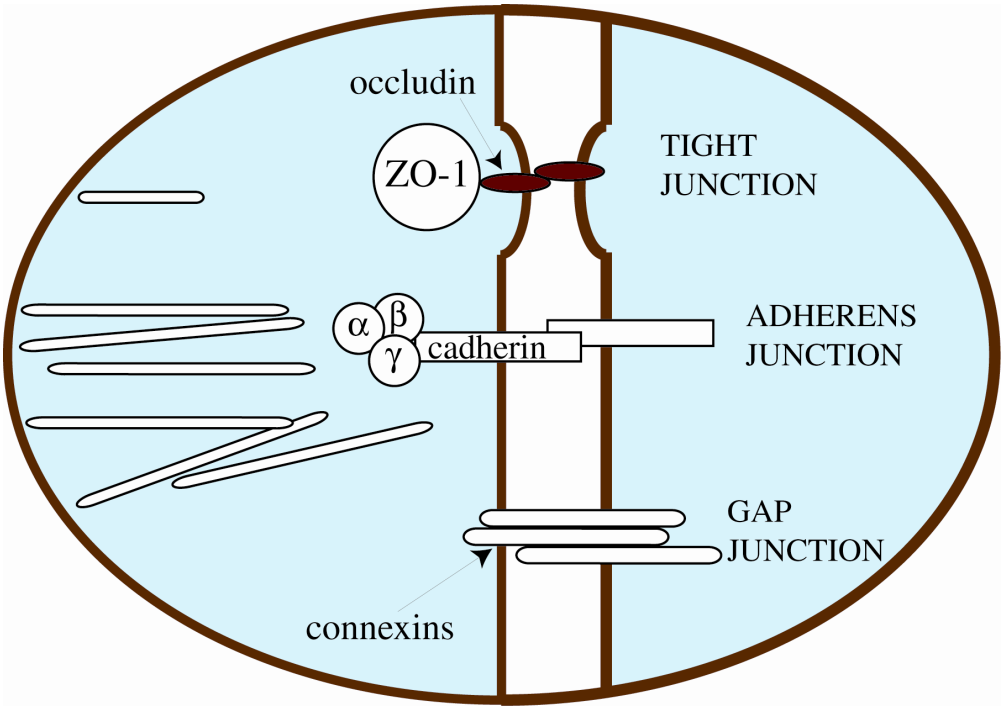

Figure **2-2**: Tight junctions, adherens junctions and gap junctions.

Tight junctions are formed primarily by a family of transmembrane proteins and occludin is the most studied [29]. Other peripherally localized cytoplasmic proteins such as ZO-1[30], ZO-2 [31], cingulin [32], 7H6 antigen [33], and symplekin [34] appear to link occludin with the actin-based cytoskeleton. The importance of tight junctions has been shown in the brain-blood barrier where brain endothelial cells with high levels of occludin expression had remarkably low permeability. In epithelium or endothelium of non-neural tissue, the expression level of occludin is much lower than that of the blood-brain barrier [35]. Although it has been established that tight junctions of HUVEC are not nearly as well developed as is blood-brain barrier EC [36], the transport across the endothelium is still regulated in large part by tight junctions [26, 35].

The formation of the tight junction does not solely depend on the presence of occludin. The disruption of actin filaments causes alterations in tight junctions. Actin-disrupting drugs such as cytochalasin have shown that any perturbation of perijunctional actin will disrupt the paracellular barrier by altering tight junctions and cell shape [37].

Taken together, tight junctions, adherens junctions and the cytoskeleton are all important in the regulation of EC permeability, but their contributions may vary in different cell lines.

2.4 Biochemical Signal Transduction Pathways

The cell membrane is an extremely active site for the cell to communicate with the changing environment. This is accomplished by receptor proteins at the cell membrane. Three classes of cell surface receptor proteins have been identified: ion-channel-linked, G-protein-linked, and enzyme-linked (Figure **2-3)**. Ion-channel-linked receptors are involved in rapid synaptic signaling excited by neurotransmitters. G-protein-linked receptors act indirectly to regulate the activity of a separate plasma-membrane-bound target protein, which can be an enzyme or an ion channel. The regulation is mediated by a trimetric GTP-binding regulatory protein (G-protein). Enzyme-linked receptors are mainly protein kinases or associated with protein kinases. When activated, either function directly as enzymes or associated with enzymes [20].

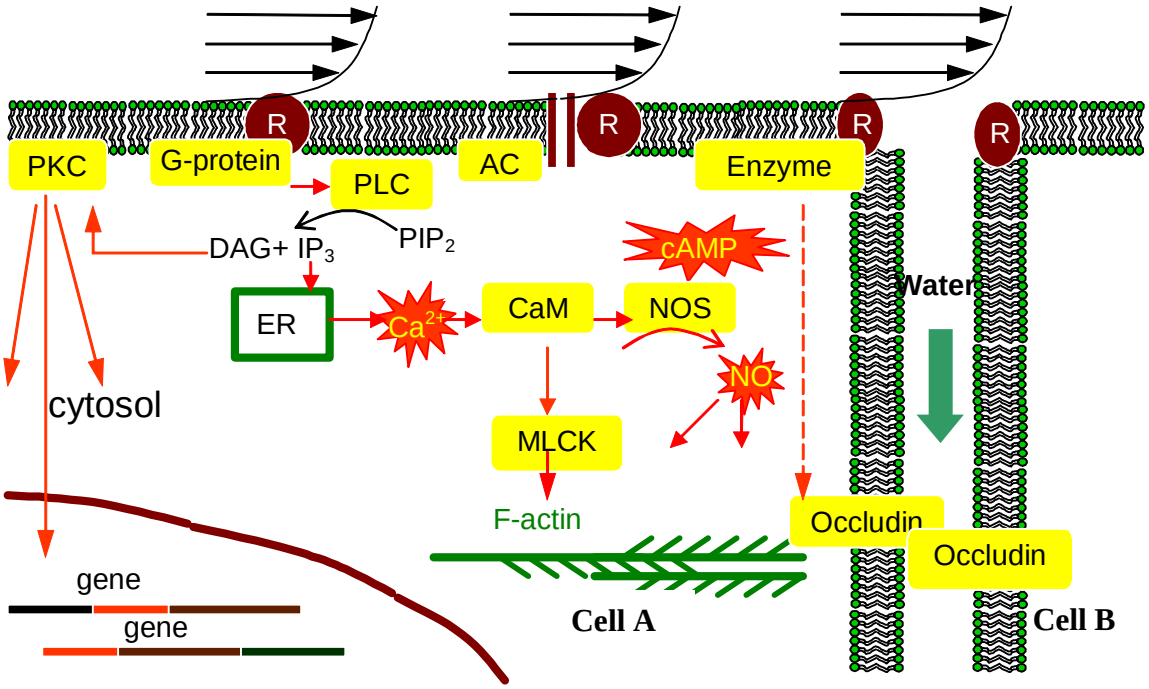

Figure **2-3**: Schematic of signal transduction pathways controlling endothelial L_P
See text for abbreviations

Shear stress, as well as other signaling molecules, could directly or indirectly act on the receptors, thereby initiating a cascade of biochemical reactions in the cell and altering the concentration of one or more small molecules (such as cAMP, calcium, and NO) referred to as second messengers. Subsequently, the second messenger activates protein kinases, leading to protein phosphorylation or gene transcription (mRNA). The total amount of target proteins and their phosphorylation states are thus altered, hence the properties associated with the proteins. Recent studies have shown that shear stress can

induce a series of cell responses. For example, shear stress activated protein kinase C (PKC) to induce platelet-derived growth factor (PGDF) gene expression[38], and open K^+ channels [39]. Shear stress can also activate a number of other gene expressions in HUVEC, such as c-fos [40], endothelin [41, 42]. Finally, it has been reported [43] that shear stress on the endothelium induced alterations in cell structure by realignment of the cytoskeleton and stress fibers.

Two of the most widely used intracellular mediators are cyclic AMP (cAMP) and Ca^{2+}. cAMP and calcium exert their effects by activating the cylic AMP dependent protein kinase (PKA) and calcium/calmodulin-kinase (CMPK). Nitric Oxide is a very unique signaling molecule. It is the most potent in causing smooth muscle cells in the vessel wall to relax. Because of this, it was originally named endothelium-derived relaxing factor (EDRF). NO also act as a second messenger in endothelium. Figure **2-3** is the schematic of the signal transduction pathways controlling EC transport properties induced by shear stress, but the picture is undoubtedly much more complicated than depicted here. The target proteins for permeability regulation are occludin and F-actin.

2.4.1 Calcium functions as a ubiquitous intracellular messenger

Calcium enters the cytosol from the extracellular fluid when calcium channels such as Ca^{2+}-K^+ ionic channels open as a result of a chemical signal or a change in membrane potential. Calcium can also be released from intracellular compartments, the

endoplasmic reticulum (ER), by inositol phospholipid (IP_3)-gated Ca^{2+}-releasing channels.

Most actions of calcium are mediated by protein phosphorylation catalyzed by a family of calcium/calmodulin-dependent protein kinases (CaM-kinases). Two mechanisms regulating permeability in EC are calcium/calmodulin dependent. First, cell retraction by the phosphorylation of myosin is accomplished by myosin light chain kinase (MLCK) which is activated by a calcium/calmodulin complex. Second, the activity of constitutive NOS (also called endothelial NOS or eNOS) is calcium/calmodulin and NADPH dependent [44]. Furthermore, it has been reported that induction of the endothelial NOS gene is calcium dependent, but not calcium-activated [45]. Therefore, a role of calcium is expected in the regulation of permeability.

Shear stress, like signaling molecules, can regulate the intracellular calcium concentration. Sigurdson [46]reported that even a gentle mechanical force perturbation (0.1 dyne/cm^2) can cause a transient rise in intracellular calcium concentration. However, for oscillatory shear stress, Helmlinger and Nerem reported that purely oscillatory shear stress (0 ± 20 dyne/cm^2) did not induce a calcium response in BAECs.There are also stretch activated calcium channels that may be stimulated by shear stress. Brakemeier S *et al.* [47] reported that laminar flow shear stress of 5 dyne/cm^2 for 4 hours can up-regulate the stretch-activated calcium channel (SAC), leading to enhancement of calcium influx in HUVEC.

Thrombin affects cell permeability through the calcium pathway [48]. Binding of thrombin with its receptor initiates activation of heterotrimeric G-Proteins, which in turn, induce a decrease in cAMP level in the cell, an increase in intracellular Ca^{2+} and

diacylglycerol concentrations, and activation of the small G-protein Rho. Then phosphorylation of myosin light chain, as a result of activation of myosin light chain kinase and inactivation of myosin phosphatase stimulates stress fiber formation and triggers actomyosin contraction, thereby increasing the permeability. This process requires a calcium signaling mechamism [49].

2.4.2 NO pathway

In the vasculature, NO plays an important role in regulating vasomotor tone by eliciting relaxation of smooth muscle cells, resulting in increased regional blood flow. NO is synthesized by the action of the enzyme nitric oxide synthase (NOS) by the deamination of the amino acid arginine. Because it diffuses readily across membranes, NO diffuses out of the cell where it is produced and passes directly into neighboring cells. It acts only locally because it has a short half-life (about 5-10 seconds). NO diffuses into target cells where it activates the cytosolic form of guanylyl cyclase and causes formation of the second messenger cGMP.

The flow-induced release of NO by endothelial cells has been demonstrated *in vitro*, *in vivo*, and in perfused vessels. Kuchan and Frangos [50]using a parallel plate flow chamber and cultured HUVEC reported that shear stress ranging from 1.8 to 25 dyne/cm^2 increased NO release in a biphasic manner, with an initial burst followed by a sustained production for 12 hours. Cultured bovine endothelial cells exposed to shear stress are reported to have elevated levels of NOS mRNA[51].

NO has been demonstrated to alter transport properties. However, the effect of NO on cell permeability is still controversial. A number of studies indicate that NO increases the endothelial transport rate. Meyer and Huxley [52]superfused sodium nitroprusside, a NO donor, into frog mesenteric venular capillaries and recorded a 2.6 fold elevation in Lp. Subsequently, Rumbaut *et al*. [53] showed that the NOS inhibitor, L-NMMA, decreased Lp using a similar experimental protocol. However, there are other studies which exhibit an opposite action of NO. Kube and Granger [54]and Kurose[55] reported an enhancement of albumin permeability when vessels were exposed to the NOS inhibitor, L-NAME, in feline small intestinal microvessels and in mesenteric venules of male Sprague-Dawley rats, respectively. Thus, the effect of NO on transport may depend on the specific species and the vascular origin of the endothelium.

2.5 Effect of shear stress on BAEC transport properties—Previous findings in our lab

Over the last decade, Dr. Tarbell's laboratory has developed an *in vitro* model in which bovine aortic endothelial cells (BAEC) were grown on porous, polycarbonate Transwell filters. This *in vitro* model has exhibited physiological transport barrier properties, namely albumin permeability and hydraulic conductivity similar to those observed in intact vessels. Some important findings related to this study are listed below.

A clear *in vitro* demonstration of a shear stress effect on BAEC permeability was first reported by Jo *et al.* [56] who showed that shear stress increased albumin permeability. Dull *et al.* [57]demonstrated that L_P depends strongly on albumin

concentration. Addition of 1% BSA into experimental media (MEM) lowered the hydraulic conductivity from 21.3 $\times 10^{-7}$ (no BSA) to 2.35 $\times 10^{-7}$ cm/sec/cm H_2O. Sill[8] then showed that shear stress (10 dyne/cm^2) resulted in a time dependent increase in which endothelial L_P increased by 2.6 ± 0.42 fold at the end of sixty minutes. Upon removal of shear stress, L_P remained significantly elevated compared to baseline Lp. Sill also reported the dose response of L_P to shear stress in the range of 0.1 – 20 dyne/cm^2 with the threshold lying between 0.1—0.5 dyne/cm^2. They also demonstrated that the response could be blocked by addition of a cAMP analogue or a phosphodisterase inhibitor, suggesting a role for cAMP in the pathway.

Chang [58]further proved that the shear-induced increase in hydraulic conductivity is mediated by a Nitric Oxide-dependent mechanism. SNAP (a NO donor) increased BAEC L_P by 2.23 ± 0.14 and 4.8 ± 0.66 fold at the end of three hours for 100 uM and 500 uM SNAP respectively. In separate experiments, BAEC exposed to the NOS inhibitors L-NMMA and L-NAME exhibited significant attenuation of the shear-induced increase in L_P in a dose-dependent manner. These lines of evidence suggested that NO is involved in the shear-L_P response. Upstream of the NO pathway, chelating extracellular calcium with EGTA (500 uM) partly attenuated the shear-L_P response, whereas chelating intracellular calcium with EGTA-AM (5 uM) had no effect in attenuating the shear-induced increase in L_P. The calmodulin antagonist, calmidazolium (CMZ 25 uM) inhibited the initial transient phase of the shear-Lp response. These data suggest that the initial increase in L_P is calcium dependent, whereas the second phase is not.

Downstream of the NO pathway, neither cGMP/PKG nor a metabolic pathway is functional in regulating hydraulic conductivity.

Hillsley and Tarbell [18]studied the effect of oscillatory shear stress on BAEC Lp. Non-reversing shear stress (10 ± 10 dyne/cm^2) increased L_P 3 fold within 90 minutes, similar to the effect of 10 dyne/cm^2 steady shear stress, whereas reversing oscillatory shear stress (10 ± 15 dyne/cm^2) had no effect in L_P. In addition, 10 ± 15 dyne/cm^2 stimulated a 14 fold increase in NO while 10 ± 10 dyne/cm^2 induced 2.9 fold in NO, implying that flow reversal was playing an important role in regulating the hydraulic conductivity.

DeMaio *et al.* [59]studied occludin phosphorylation under steady shear stress in BAECs. 10 and 20 dyne/cm^2 shear stress significantly reduced occludin in a time-dependent manner such that 3 hour exposure to shear reduced occludin content to 44% and 50% of control, respectively, while the corresponding L_P increased by 4.7 fold after 3 hours. Shear stress also increased occludin phosphorylation after 5, 15 , 30, and 180 minutes, suggesting that alternations in the occludin phosphorylation state and occludin total content are potential mechanism for shear to increase L_P in BAEC.

2.6 Specific Aims of This Study

1. To determine the forces that determine Starling's law and validate our *in intro* model. We have hypothesized that it is local concentrations, not the global concentrations (interstitium and blood concentration), that determine the Starling's forces.
2. To determine the effects of steady and oscillatory shear stress on the hydraulic conductivity (Lp) of HUVEC. We will culture HUVEC monolayers on porous filter and measure Lp in response to steady shear stress and oscillatory shear stress (with or without reversal) in a unique apparatus developed in our lab. This specific aim will complete the data base of transport responses of HUVEC, which seem to respond differently than BAEC.
3. To determine the physical transport pathways that are affected by shear stress. We hypothesize that occludin is a possible determinant of permeability, and that shear stress regulates occludin at the transcriptional level (mRNA and protein expression) or at the post-translation level through phosphorylation.
4. To determine the biochemical mechanism that mediates the effect of shear stress on EC transport. We will conduct experiments using activators and inhibitors of biochemical pathways (calcium pathway and nitric oxide pathway) within cells to probe for the mechanism underlying the shear stress responses of HUVEC.

Chapter 3

Chemicals and Methods

3.1 Chemicals

The following chemicals were obtained from Sigma Chemical (St. Louis, MO): bovine serum albumin (BSA) (30% solution, fraction V), minimal essential media (MEM), minimal essential media without phenol red (MEM w/o phenol red), protein standard (bovine serum albumin), nitrate reductase (EC1.6.6.1), gelatin (type A from porcine skin), L-glutamic acid, fibronectin (cell culture grade from bovine plasma, lyophilized), penicillin-streptomycin solution, S-nitroso-n-acetyl-penicillamine (SNAP), N^G-methyl-L-arginine monoacetate salts (L-NMMA), sulfanilamide, N-(1-napthtl)ethlenediamine (NED), β-NAD phosphate reduced form (β-NADPH), flavin afenine dinucleotide disodium (FAD), sodium nitrate(Sigmal Ultra), sodium nitrite, sodium bicarbonate, HEPES, trypsin-EDTA solution, benzamidine, 2,3-diaminoanphathalene (DAN), acetic acid (glacial)

Fetal bovine serum (FBS) was obtained from Hyclone (Logan, UT). Collagenase A (EC 3.4.24.3) (>0.15 Wunsch units/mg) and Blenzyme 2 were purchased from Roche (Indianapolis, IN). Calf intestinal alkaline phosphatase (CIP) was obtained through New England BioLabs (Beverly, MA)

1,2-bis(*o*-aminophenoxy)ethane-*N*,*N*,*N'*,*N'*-tetraacetic acid (BAPTA-AM) and calcein AM were obtained from Molecular Probes (Eugene, OR), Hank's balanced salts

w/ phenol red, w/o calcium and magnesium (HBS) and phosphate buffered saline (PBS) were obtained from Irvine Scientific (Santa Ana, CA), Endothelial Growth Medium (EGM) (Endothelial cell basal media supplemented with EGM singlequoet with final concentrations of 0.1% GA-1000, 0.4% BBE, 0.1% hydrocortisone, and 2% FBS) was obtained from Clonetics (Walkersville, MD). Transwell polycarbonate/polyester filter (0.4 μm pore size, 24.5 mm diameter) were obtained from Costar Corporation (Cambridge, MA).

The following products were used for gel electrophoresis and Western blotting. Protein DC method kit (reagent S, reagent A and reagent B), glycine, *N*,*N*,*N*,*N*-tetra-methyl-ethylenediamine (TEMED), PVDF membrane (size=0.2 um), sodium dedecyl sulfate (SDS), Acrylamide/Bis 30% solution, Tris(hydroxymethyl)-aminomethane, ammonium persulfate, and precision molecular weight marker were obtained from Bio-Rad (Hercules, CA). Rainbow molecular marker and ECL Western blotting analysis system were obtained from Amersham Pharmacia Biotech (Piscataway, NJ). Kodak X-Omat Blue film was obtained from NEN Life Science Products (Boston, MA). Polyclonal rabbit anti-occludin was obtained from Zymed Laboratory (San Francisco, CA). 3-(cyclohexylamino)-propanesulfonic acid (CAPS) was obtained from Calbiochem (San Diego, MA). Methanol was from J T Baker (Phillisburg, NJ). 1,1'-dioatadecyl-3,3,3',3'-tetramethyl-indocarbocyanine perchlorate-acetylated low density lipoprotein (DiI-Ac-LDL) was obtained from Biomedical Technologies Inc. (Stoughton, MA)

3.2 Cell Culture

3.2.1 Cell culture of BAECs

Endothelial cells were either harvested from bovine thoracic aortas and cloned, or purchased from VEC Technologies, Inc. (Rensselaer, NY). Cells were cultured in MEM supplemented with 10% FBS, 50 U/ml penicillin, 50 ug/ml streptomycin and 2 mM L-glutamine as described previously[60]. Cells were split 1:3 for the subculture every 3 to 4 days. In order to freeze cells, 1 ml of freeze down solution (MEM/10% DMSO/20% FBS) instead of normal media (MEM-10% FBS) was used and cells were put into a freezer vial at a density of 750,000 cells/vial. Cells were kept at –20 ^{o}C for about 2 hours, and then transferred to –80 ^{o}C overnight and finally kept at -180 ^{o}C. Cells of passage 8-11 were used in the experiments.

3.2.2 Primary culture of HUVECs

A total of sixty-five primary cultures were used during this study. Human umbilical cords were collected from the Hershey Medical Center. Human umbilical vein endothelial cells were isolated by the method of Jaffe et al[61]. Briefly, cells were obtained by incubating for 35 minutes with 0.5—2.5 U/ml collagenase A (the best working concentration must be optimized for each lot) or Blenzyme 2 (0.3- 0.5 Wunsch units/ml). Longer incubation time lowered cell viability and impaired cell function. Cells were fed every 2 days with EGM media supplemented with 10% FBS, and seeded onto

Transwell filters or slides. Cells of passage 2—4 were used in the experiments. Some difficulties with HUVEC cultures are discussed in section **3.8.**

3.3 Identification of Endothelial Cells by Flow Cytometry

Vascular endothelial cells were identified by the typical 'cobblestone" morphology exhibited by confluent monolayers, and by their ability to take up acetylated low-density lipoprotein (Ac-LDL). The cells were incubated with 10 ug/ml of DiI-Ac-LDL at 37 ^{o}C for 4 hours. Subsequently, cells were dislodged by trypsin. The suspended cells were subjected to flow cytometry at the Center for Cell Quantitative Analysis, Penn State University. Appendix B shows the results. At passage 5, cells were 92.5% pure (average of 2 sortings). Since contaminating cells outgrow endothelial cells, purity of cells at passage 2 to 4 should be higher than this.

3.4 Filter/Slide Preparation.

For hydraulic conductivity studies, both polycarbonate (opaque) and polyester (clear) filters have been used, because both filter types provide only one thousandth of the resistance of cell monolayers and no apparent difference in cell function has been observed. Filters were first treated with 0.5% acetic acid for 20 minutes at 56 ^{o}C, followed by an hour in 5 mg/ml gelatin. Filters were finally disinfected by ultraviolet light overnight. The filters were then precoated with 1 ml of 30 ug/ml fibronectin for at least 1 hour. BAECs were seeded at a density of 2.5×10^5 cells/cm^2 and a minimum

hydraulic conductivity was reached 7 to 9 days post-seeding. HUVECs were seeded at a density of 1~2 × 10^5 cells/cm^2, and a minimum hydraulic conductivity was reached 5 to 9 days post seeding. For the analysis of NO production, filters were cut away from Transwell inserts and the inserts were glued onto glass slides washed in a boiling sodium bicarbonate solution. Sterilized slides were then pretreated with fibronectin for 1 hour. Cells were seeded on glass slides at a reduced density (two thirds of the density for filters), because cells on glass slides grew faster than they did on filters. Cells generally took 2~3 days to reach confluency, and they were used immediately for experiments.

3.5 Visualization of Endothelial Monolayers

Selected monolayers on polycarbonate filters were visualized for damage after exposure to the various experimental treatments. The fluorescent indicator calcein AM was used to check for cell viability. Briefly, monolayers were rinsed with PBS, followed by incubation in 0.005 mg/ml calcein AM for 15 minutes at 37 ^oC. An Olympus IMT-2 inverted microscope was used to visualize the cell monolayer at excitation of 480 nm and emission of 535 nm. Viable cells were stained in green and viewed at a magnification of 100×. Micrographs were taken by using an Olympus DP11 microscopic digital camera.

3.6 In Vitro Method of Applying Defined Shear Stress

Shear stress was applied by the parallel-disk system which consisted of a rotating disc oriented parallel to and separated by a known distance h from a stationary surface covered with cells. The magnitude of shear stress τ at radius r is given by Eq. **3.1**

$$\tau = \frac{\mu \cdot \omega \cdot r}{h} \qquad \textbf{3.1}$$

where μ is the viscosity, ω is rotation speed (rpm), and h is the gap distance between the disk and the filter. Shear stress increases from zero at the center to the maximum at the edge of the filter. The average shear stress over the entire filter area is two thirds of the maximum. In this study, the shear stress value is reported as the maximum value. It should be noted, however, that if the dependence of L_P on shear is nonlinear, the spatial variation of shear stress in the apparatus will provide some distortion in the measured shear dependence based on the maximum value. There also exists a shear gradient in the radius direction at 8.3 dyne/cm^2/cm when the shear stress is 10 dyne/cm^2. However, this shear gradient is insignificant when compared to the shear gradient on each cell surface which is at the order of 1 dyne/cm^2/um [85]. The oscillatory shear stress is given by a simple sinusoidal waveform (Eq. **3.2**).

$$\tau = \tau_{steady} + \tau_{oscillatory} \cdot \sin(2\pi \cdot f \cdot t) \qquad \textbf{3.2}$$

where f is the frequency. In our experiments, a physiological frequency of 1 Hz was used all the time, and the shear stress is denoted as $\tau = \tau_{steady} \pm \tau_{oscillatory}$.

3.7 Measurement of Volume Flux

A detailed description of the experimental apparatus used to measure volume flux was presented in Sill, et al.[8]. Figure **3-1** shows the schematic of the experimental apparatus. Briefly, the entire apparatus was housed in a Plexiglas box and kept at an ambient air temperature of 37 ºC. The polycarbonate membrane Transwell filter which contained the BAEC monolayer was sealed within a two-piece polycarbonate assembly that separated the luminal (monolayer side) and abluminal compartments. A 5% CO_2 - 95% air gas port provided continual positive pressure outgassing and maintained pH at 7.4. The abluminal chamber was attached by Tygon tubing to a borosilicate glass tube followed by additional Tygon tubing to a reservoir. The difference in level of the fluid in the luminal compartment and in the reservoir provided an adjustable hydrostatic pressure head (ΔP) which acted as a driving force for fluid movement. The experimental media was MEM with 1% BSA and no FBS.

For the measurement of water flux, an air bubble was introduced into the medium in the borosilicate glass tube and bubble movement, indicative of volume flux, was measured using a custom designed tracking device interfaced to a computer. The tracking unit consisted of a traveling spectrophotometer that recorded the bubble's displacement versus time, allowing calculation of volumetric flow rate as follows:

$$Jv = (\Delta d / \Delta t) \cdot F \qquad \textbf{3.3}$$

where $\Delta d / \Delta t$ is bubble displacement per unit time and F is a tube calibration factor (i.e. fluid volume contained in a known length of tubing). Because a bubble tracker could

follow bubble motion in one direction only, two bubble trackers were used to measure bubble motion in opposite directions simultaneously so that a change in flow direction (reabsorption) could be detected when luminal pressure was dropped below osmotic pressure suddenly.

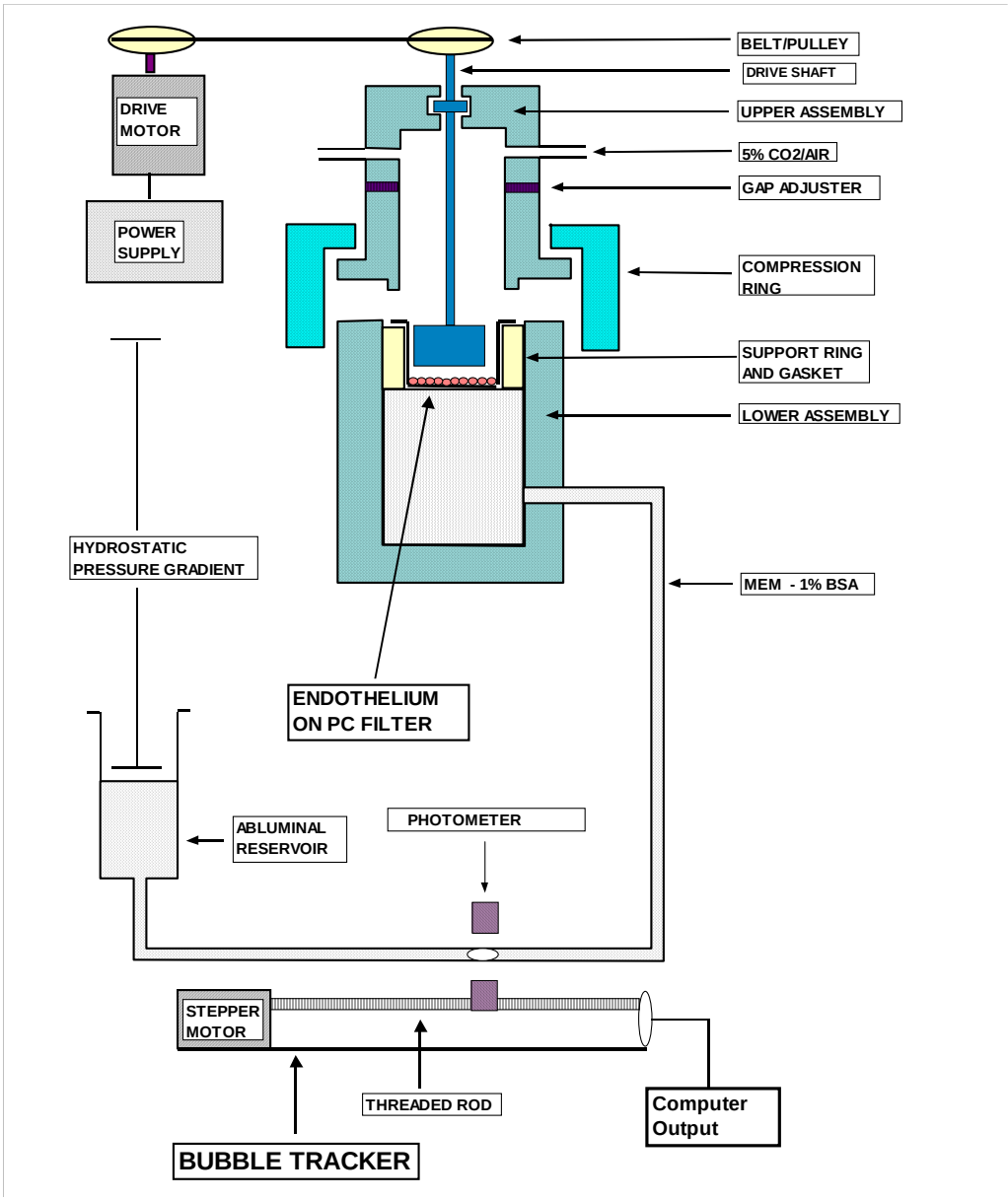

Figure **3-1**: Schematic of apparatus to impose shear stress on an endothelial monolayer to measure hydraulic conductivity (L_p)

3.8 Difficulties in HUVEC Cell Culture and Baselines at 10 cm H_2O

In HUVEC experiments, the pressure differential was fixed at 10 cm H_2O, and MEM-1% BSA experimental media was added to both the luminal and abluminal sides of the filter, thus minimizing any possible osmotic pressure differential described by equation 2.4. Starling's law therefore simplifies to:

$$Jv / A = L_P \cdot \Delta P \qquad \textbf{3.4}$$

In this case, volume flux (Jv / A) is proportional to hydraulic conductivity (L_P).

Due to the existence of giant cells, a stable and low hydraulic conductivity of the cell monolayer was quite difficult to obtain. Figure **3-2**A shows a representative experiment with some giant cells on the cell monolayer. The volume flux at the beginning of the experiment was reasonable at 4.18 $\times 10^{-6}$ cm/sec, but it kept increasing during the experiment. At time 55 minutes it was already 9.02 $\times 10^{-6}$ cm/sec and at time 100 minutes volume flux jumped to 6.87 $\times$ 10^{-5} cm/sec (more than 10 fold increase compared to volume flux at time 0). Figure **3-2**B shows a typical view of the filters using calcein AM staining. Some "giant cells" about 100 nm long embedded inside normal endothelial cells formed a leaky area that was the cause for high baseline. The normal diameter of HUVEC averages 15 nm, about 4 nm longer than that of BAEC (measured by ImagePro-Plus software). Coverage with these giant cells as low as 5% could exert a damaging effect on HUVEC baseline. This dramatic increase caused by giant cells can shield other cell responses. In order to differentiate the effects of cell responses and those of "giant cells", control experiments with 10 cmH_2O pressure differential only had to be performed simultaneously in each set of experiments, and only sets of experiments with

stable control baselines (showing volume flux with less than two fold increase by the end of the experiment) were considered valid data.

Figure **3-3B** shows a normal cell monolayer with no "giant cells". A tight monolayer was clearly formed, corresponding to a low baseline. It should be noted that these cells were harvested using Blenzyme 2. Figure **3-3A** shows the average normal baselines of HUVEC with few "giant cells" isolated using either collagenase A or Blenzyme 2, respectively. The first 60 minutes show a decrease in L_P. This decrease is termed a "sealing effect". It has been shown to occur repeatedly and is thought to be due to mechanical pressurization as well as cell responses to transmural flow. In order to eliminate the difference between monolayers, all Lp values were normalized by the Lp value at time 55 minutes. Baselines using collagenase A showed a Lp of $1.62 \pm 0.26 \times 10^{-7}$ cm/sec/cm H_2O (n=8) at 55 minutes, which was lower than the Lp of $3.20 \pm 0.58 \times 10^{-7}$ cm/sec/cmH_2O (n=16) using Blenzyme 2. Collagenase A showed no drifting of baselines at all. However, the quality of collagenase A varied from lot to lot. The stable and low baselines shown in Figure **3-3** were obtained from one particular lot of collagenase A with a low ratio of trypsin to specific activity. Other lots did not show these stable baselines. The effect of components of collagenase A on HUVEC baselines is shown further in Table **3-1**. Blenzyme did not vary from lot to lot, and was primarily used in HUVEC primary cultures. On average, Blenzyme is better than collagenase A.

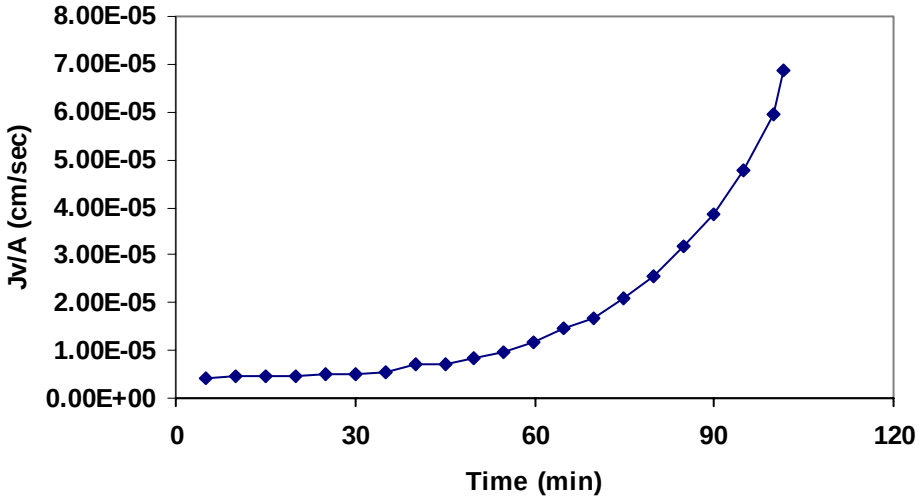

(A)

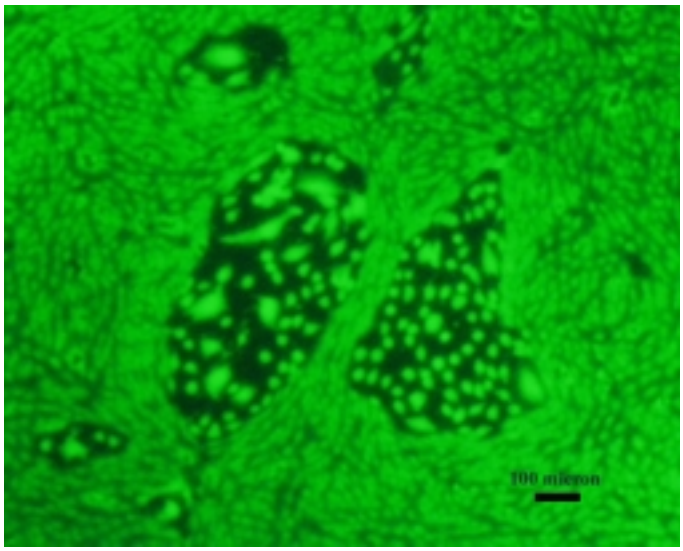

(B)

Figure **3-2**: Cell monolayer with some "giant cells" and its corresponding baseline.

(A): A representative drifting baseline. 10 cm H_2O hydrostatic pressure was applied at time 0. Jv/A increased from 4.18×10^{-6} cm/sec at the beginning to 6.87×10^{-5} cm/sec at time 100 minutes (an increase of more than 10 folds). (B). The calcein staining of the filter with a hydraulic conductivity on (A) showed some "giant cells" embedded inside normal endothelial cells, forming a leaky area that leads to a drifting and high baseline.

(A)

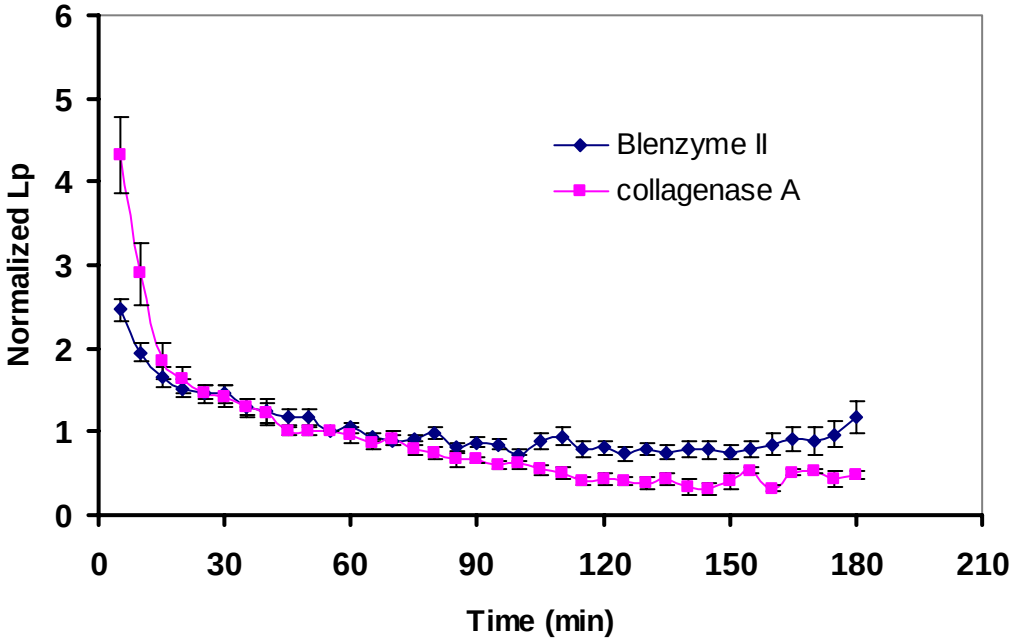

(B)

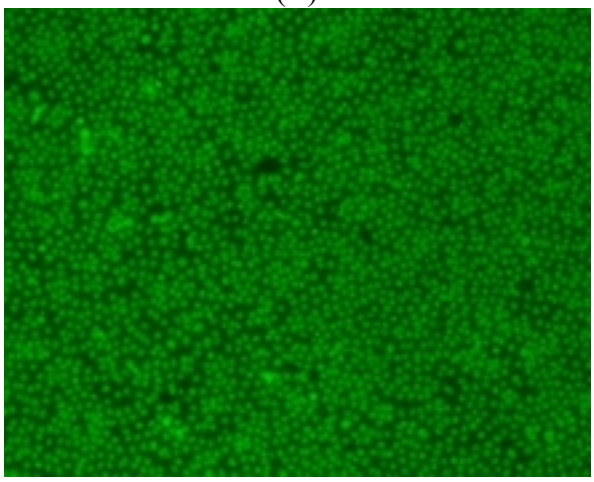

Figure **3-3**: HUVEC baselines at 10 cm H_2O hydrostatic pressure using collagenase A and Blenzyme 2.

(A): 10 cm H_2O hydrostatic pressure was applied at time 0, and experiments were run for 180 minutes. The average L_P values for collagenase A were 1.62 ± 0.26 × 10^{-7} cm/sec/cm H_2O (n=8) whereas L_P values for Blenzyme 2 were 3.20 ± 0.58 ×10^{-7} cm/sec/cmH_2O (n=16)
(B): Endothelial cells on filters using calcein-AM staining

Culturing of HUVEC is much more challenging than that of BAEC because of the following reasons:

1. "Giant cells" are more prominent in HUVEC than BAEC. The presence of a few "giant cells" makes the whole cell monolayers more permeable. They disrupt the normal cell function as a barrier, causing a leaky area around them. Although the exact cause of these cells remains unknown, they are believed to be mutated ECs stemming from the incubation with collagenase or blenzyme. As for BAECs, we did not observe any giant cells on the filters.

2. The quality of HUVEC monolayers is very sensitive to the components of the collagenase used to isolate them. Collagenase A is a mixture of proteases. The quality of collagenase varies a lot in terms of specific activity and the activity of neutral proteases (Table **3-1**). Only good quality collagenase yielded a successful cell line to work with. The major contaminants are trypsin, caseinase, and clostripain. From the table, it is very clear that the ratio of trypsin to specific activity is highly correlated to the cell quality, and a low value is desired. Blenzyme 2 is also a mixture of highly purified collagenase and neutral protease enzymes, but with a consistent composition.

3. Only low passage of HUVEC (up to 4) can be used in experiments, as opposed to passage 12 for BAEC. As shown in Figure **3-4**, the average Jv/A values of passage 2 to 4 showed a slight difference. However, for cells at higher passages, not only was the average Jv/A higher than 5×10^{-6} cm/sec, the physiological value, but it was unstable and drifted up more than 3 fold by the end of

experiments. In addition, calcein AM staining showed more giant cells at higher passages. The splitting ratio is as important as passage numbers. For HUVEC, it is suggested to maintain this ratio at 1:2, although sometimes 1:3 can be used if cells grow fast and reach confluence in just 2 days.

4. HUVECs demand high quality FBS for normal function. Because of this property, HUVECs are used to screen serum samples in our lab.

Table **3-1**: **Effect of collagenase composition on primary culture cells**

Cell quality	***5***	***4***	***3***	***2***	***2***	***1***
Specific activity(25C)	0.49	0.34	0.36	0.23	0.45	0.17
Contaminants						
Trypsin(25C, BAEE as substrate.)	0.12	0.09	0.11	0.1	0.25	0.25
Caseinase (25C,Casein as substrate)	535	375.6	266	830	187.2	424
Clostripain (25C, BAEE sub., DTT act.)	2.58	0.8	0.63	3.2	1.3	3.5
Ratio of trypsin to specific activity	0.245	0.265	0.306	0.435	0.556	1.471

Unit in U/mg

Note: Cell quality is rated by monolayer hydraulic conductivity properties on a scale from 1 to 5, where 1 represents a high and drifting baseline and 5 represents a low and stable baseline.

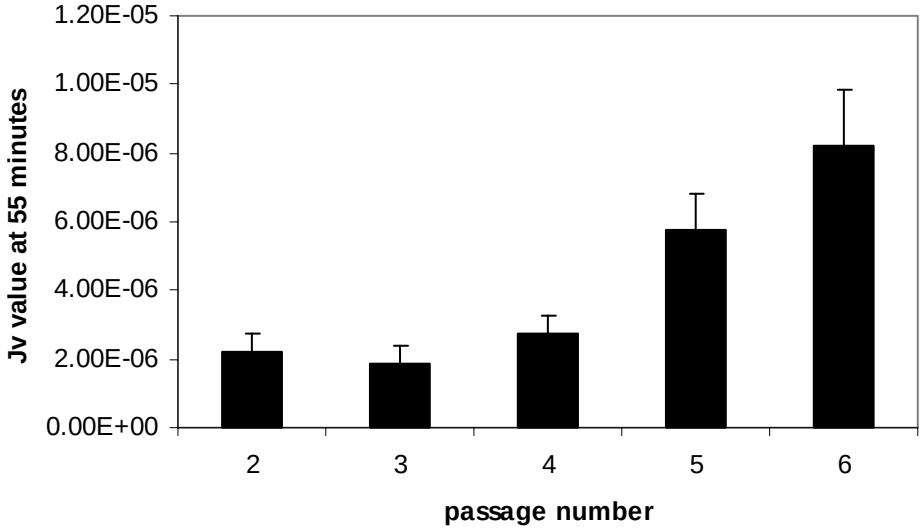

Figure **3-4**: Effect of passage number on HUVEC baseline Jv/A

Cells at passage numbers of 5 and 6 have an average Jv/A values higher than 5×10^{-6} cm/sec at a pressure differential of 10 cmH_2O. Cells at passage numbers between two and four yield an average Jv/A value less than 5×10^{-6} cm/sec. There is a significant difference between cell passage number 4 and 5 (P=0.012)

Taken together, for a successful primary culture, high quality collagenase A and FBS is critical. When good quality collagenase A is unavailable, Blenzyme 2 can be used. Cells should be split at a ratio of 1:2, and only cells up to passage 4 can be used for experiments.

3.9 Determination of Nitric Oxide Concentration

Nitric oxide was assayed indirectly by measuring its stable degradation products, nitrate (NO_3^-) and nitrite (NO_2^-). To measure nitrate concentration, it has to first be reduced to nitrite by nitrate reductase. 50 ul of sample was mixed with 4 ul of enzymatic mixture (2 U/ml reductase, 50 uM β-NADPH and 5 mM FAD) and 5 ul of 920 mM KH_2PO_4 buffer (pH 7.5), and incubated at 37 ^oC for 3 hours to convert nitrate to nitrite. Nitrite reacts with Griess reagent to produce diazochromromophore, which can be accurately measured by its absorption at 540 nm [62]. Then 40 ul of freshly made 2.3% sulfanilamide (dissolved in 2.3 N HCl)/ 0.93% NED mixture (72:28) was added, and absorbance was read 30-45 minutes later by microplate autoreader (Biotek Instruments). In addition, nitrite can also react with DAN to form the highly fluorescent product 1-H-naphthotriazole [63]. After the reduction step, 10 ul of fresh DAN solution (0.05 mg/ml in 0.62 N HCl) was added to each well and refrigerated at 4 ^oC for 10 minutes. Next, 10 ul of 2.8 N NaOH was added to terminate the reaction. Fluorescent readings were obtained using a Packard FluoroCounter fluorometer with excitation at 360 nm and emission at 425 nm.

Phenol red was omitted to make a standard curve because it interfers with the reading of the absorbance and fluorescence. Sodium nitrate was dissolved in either MEM w/o phenol red or MEM w/o phenol red—1% BSA at known concentrations,. The standard curves using both media are shown in Figure **3-5.**

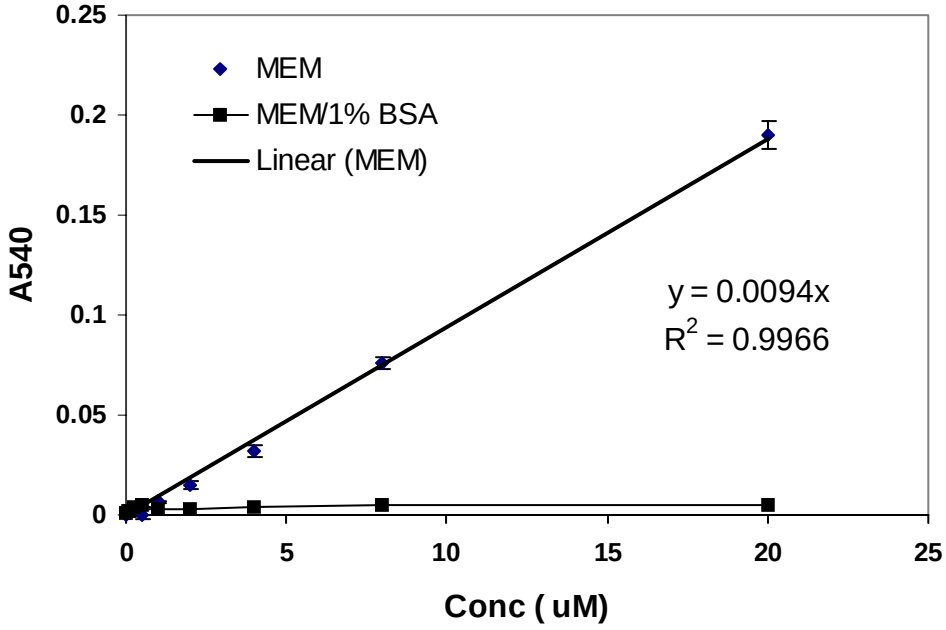

Figure **3-5**: Standard curve using nitrate in the presence and absence of 1% BSA using colorimetric method

In the absence of 1% BSA, absorbance was linear to nitrate concentration, indicating nitrate reductase had reduced all NO_3^- to NO_2^- (R^2=0.9966). However, in the presence of 1% BSA, the readings for absorbance were extremely low, suggesting nitrate reductase did not convert $NO_3^-$to NO_2^-. However, 1% BSA is actively involved in forming the barrier function of endothelial monolayers, and hence has to remain in the experimental media. Therefore, in the presence of 1% BSA, we could only measure NO_2^-. By assuming that the ratio of nitrate to nitrite keeps constant in one cell line, we use nitrite concentration as an indicator of NO concentration. In the smooth muscle cells, the nitrite contributed to 75% of total NO_x. It should be noted that the inhibition of 1% BSA on nitrate reductase was also observed in the fluorescent method (data not shown).

Figure **3-6** is a standard curve obtained by using known concentrations of nitrite in 1% BSA experimental media and the fluorescent method. A linear relation was obtained between the absorbance and concentrations. The florescent method can measure nitrite concentration down to 10 nM.

To measure nitrite concentration under various shear stresses, cells were seeded and grown to confluency on Transwell inserts glued onto glass slides. 2 ml of MEM w/o phenol red -- 1% BSA solution was added to the luminal side. The inserts were then attached to the upper shear assembly of the Lp apparatus by placing the slide on a riser and fitting it into the shear apparatus. After shear was initiated, 0.3 ml of sample was taken out at time 0, 15, 30, 60, 120, and 180 min, and an equal volume of fresh experimental media was replaced. Because of dilution (0.85), the final concentration of the solution was adjusted by the dilution factor after each sample was taken. The media samples were assayed for nitrite using the Greiss method or fluorescent method as described before[62, 63]. To convert measured sample concentration (uM) to the normalized units (nmol/mg protein) presented in Results, we multiplied by the volume of media on top of the cell monolayers (2 ml) to determine the number of moles present, and then divided by total amount of protein on slides (about 0.1 mg, as determined by Protein DC method in the following section)

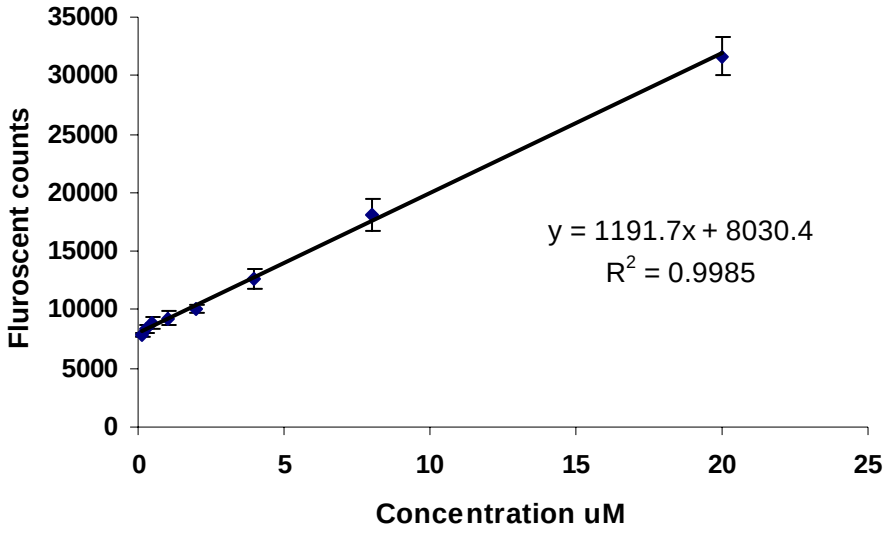

Figure **3-6**: Standard curve using fluorescent method and nitrite as standard dissolved with 1% BSA

3.10 Gel Electrophoresis and Immunoblotting

3.10.1 Quantification of protein using Protein DC method

The Protein DC method (Bio-Rad) is a modified Lowry assay [64]for protein concentration determination, especially for samples treated by detergent solubilization. The assay is based on the reaction of protein with an alkaline copper tartrate solution and folin reagent. Color development is primarily due to the amino acids, which have a characteristic blue color with a maximum absorbance at 750 nm. Briefly, 5 ul of sample or standard BSA solution was added to a 96 well plate, followed by 25 ul of reagent A' (20 ul of reagent S was added to 1 ml of reagent A to make reagent A') and 200 ul of

reagent B. The absorbance can be read at 750 nm after 15 minutes using microplate autoreader (Bio-Tek Instruments).

Figure **3-7** shows a linear relation between absorbance and concentration using BSA as a protein standard. The assay was very accurate and reliable. The average slope of standard curves was 0.17 ± 0.01 (n=8).

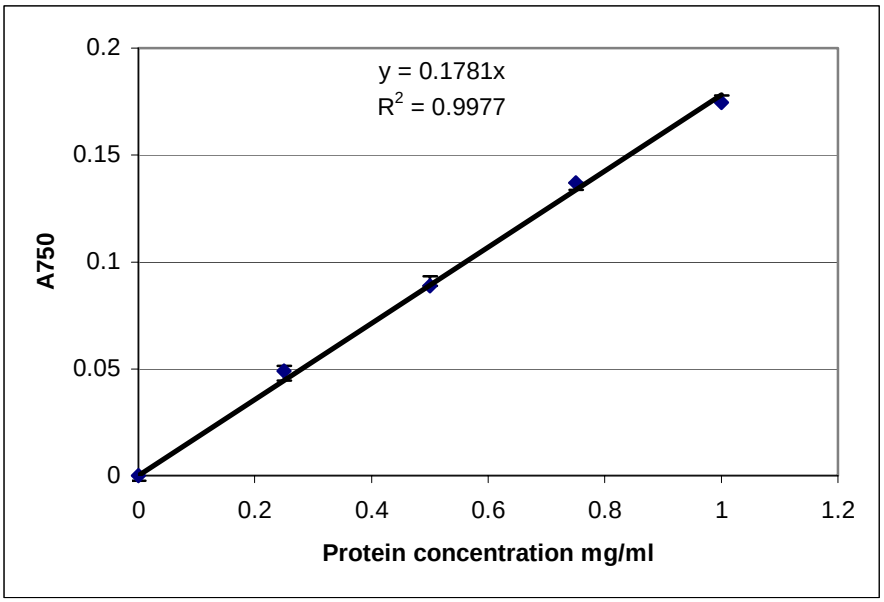

Figure **3-7**: Standard curve of BSA concentration

3.10.2 Cell extraction

Cell cultures were briefly rinsed three times with ice-old PBS and extracted with 100 ul of Stuart's lysis buffer (0.1% SDS, 0.5% Triton X-100, 0.25% deoxycholic acid, 50 mM NaCl, 1 mM EDTA, 5 mM HEPES, 10 mM NaF, 1 mM Na_3VO_4, 1 mM benzamidine, 1 mM PMSF, one tablet of Protease inhibitor cocktail, pH 7.5). The

concentration of cell lysate was determined by Protein DC method. About 1 mg/ml was the average concentration for the lysate. In order to dephosphorylate the sample, 50 ul of sample after cell extraction was treated with 25 unit of CIP (by manufacture's suggestion), and incubated at 37 ^{o}C for 1 hour.

3.10.3 Gel electrophoresis and immunoblotting

Cell lysate or cell lysate after alkaline phosphatase treatment was boiled for 5 minutes to allow proteins to denature, forming a linear structure. The denatured protein lysate was resolved by one-dimensional SDS-PAGE as described by Laemmli [65]. An 8% polyacrylamide gel with a thickness of 1 mm (the compositions for 10 ml of separating gel were as follows: 4.6 ml H_2O, 2.7 ml 30% Acry-Bis, 2.5 ml Tris, pH 8.8, 0.1 ml 10% SDS, 0.1 ml 10% AP, and 0.006 ml TEMED) yielded the best separation for occludin. A Protean II electrophoresis apparatus (Bio-Rad) was used for the separation of proteins by their molecular weights. Tris-glycine buffer (25 mM Tris, 250 mM Glycine, 0.1% SDS, pH 8.3) was used during the electrophoresis at a constant current of 45 mA/gel for 3 hours. Next, the gel was equilibrated in a transfer buffer (100 mM CAPS, 10% methanol, pH 11) and electrophoretically transferred to a PVDF membrane at a constant voltage of 10V. This membrane was blocked with 5% milk for non-specific binding in Tris-buffered saline and immunoblotted with a rabbit polyclonal anti-occludin (1:2500) followed by an anti-rabbit alkaline phosphatase-linked secondary antibody. Occludin was detected by using an enhanced chemiluminiscent kit (Amersham Pharmacia Biotech; Piscataway, NJ). The occludin bands were captured on Kodak O-mat

film. The band intensity representing the amount of protein was quantified by Image-Pro Plus Software (Media Cybernetics, Inc.). Figure **3-8** shows an example of intensity measurement from one lane of a gel. Each peak represents a protein at a different molecular weight, and the amount of protein is proportional to the area of the peak which can be automatically integrated by the computer). The background intensity is set to zero. A precision molecular marker and rainbow molecular marker were used for the determination of the molecular weight of occludin.

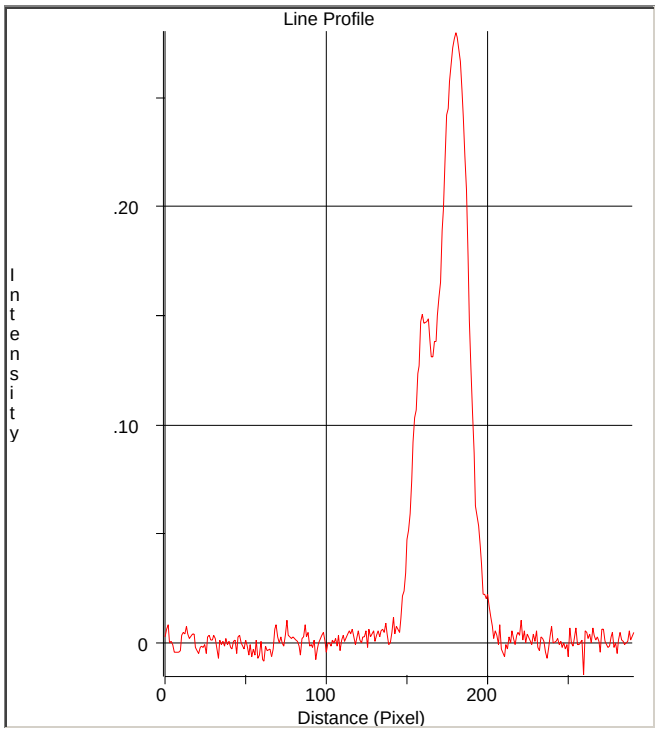

Figure **3-8**: Determination of amount of protein using Image-Pro Plus

Each peak represents a protein whose molecular weight is determined by the location of peak (migration in pixel or cm). The area of the peak is proportional to the amount of protein. Occludin phosphorylation ratio is determined by the area of peak 1 (the phosphorylated band) and the area of peak 2 (the dephosphorylated band)

3.11 Experimental Protocols

3.11.1 Changing osmotic pressure differential at fixed hydrostatic pressure differential

At the beginning of an experiment, MEM supplemented with 1% BSA (MEM-1% BSA), was added to the luminal and abluminal chambers to minimize the osmotic pressure differential. Only 1.5 ml was added to the luminal side. A hydrostatic pressure differential was not applied at this stage. After a one-hour equilibration period, a 5 cm H_2O, 10 cm H_2O or 20 cm H_2O pressure differential was gradually imposed across the monolayer over a 1 minute time interval and volumetric flow rate was recorded by the bubble tracker for 2.5 hours. The first hour was required to obtain a stable baseline value of Jv. At 60 minutes, 1.5 ml of MEM-10% BSA was added to the luminar chamber, providing a mixed luminal concentration of 5.5% BSA to initiate the osmotic pressure difference. The experiments were then conducted for 1.5 more hours.

3.11.2 Changing hydrostatic pressure differential at fixed osmotic pressure differential

In another set of experiments, after the one-hour equilibration period, 1.5 ml MEM-10% BSA was added to the luminal chamber while a 20 cm H_2O hydraulic pressure differential was imposed almost simultaneously. But after 60 minutes, the abluminal reservoir was smoothly raised up 15 cm over a 1 minute time interval, reducing the hydrostatic pressure differential from 20 cm to 5 cm H_2O (still a positive pressure drop). The movement of the bubble was monitored for another 1.5 hours. The

same protocol with 1% BSA in both the luminal and abluminal chambers was used as a control.

3.11.3 Imposing negative hydrostatic pressure differential

In order to drive steady state transmural flow from the abluminal to the luminal compartment (negative flow or reabsorption), MEM-1% BSA was placed in both the luminal and abluminal compartments, and after a 1 hour equilibration period, 10 cm H_2O hydrostatic pressure differential was applied to the monolayer for 1 hour. Then the abluminal reservoir was raised over a period of 1 minute to obtain –2, -4, and –10 cm H_2O pressure differentials, each level being held for 20 minutes. Finally, the +10 cm H_2O condition was restored and the final value of Lp was compared to the initial value at +10 cm H_2O.

3.11.4 Application of various shear stress levels to endothelial cell monolayers

After one hour of equilibrium time, 10 cm H_2O hydraulic pressure was applied to drive the transmural flow. 1 hour period was allocated to obtain a steady baseline because of the sealing effect. At time 60 minutes, steady shear stresses of 20, 10, and 5 dyne/cm^2, pure oscillatory shear stress of 0 ± 20 dyne/cm^2 , or combined steady and oscillatory shear stress of 10 ± 15, 10 ± 10, 10 ± 5 dyne/cm^2 was initiated and kept for another 2 hours.

3.11.5 Application of thrombin to cell monolayers

Thrombin was dissolved directly into experimental media. 2 ml of experimental media was used at the beginning of the experiment and 10 cm H_2O hydraulic pressure was applied to drive the transmural flow. At time 60 minutes 2 ml of 2 U/ml or 4 U/ml thrombin was added to the experimental media in the luminal side, yielding a final working concentration of 1 U/ml or 2 U/ml, respectively. The experiments were conducted for another two hours.

3.11.6 Application of 10 uM BAPTA –AM to cell monolayers

BATPA-AM came in an 1 mg bottle and was dissolved in 130 ul DMSO (solubility: 2.5 mg/100 ul DMSO), yielding a stock solution of 10 mM. It was further diluted with experimental media (MEM-1% BSA) to give a working concentration. For the hydraulic conductivity experiments, 2 ml of experimental media were used in the luminal side of the chamber at the beginning of the experiment. 10 cm H_2O hydrostatic pressure was applied at time zero. 2 ml of 20 uM BAPTA-AM was added to the luminal chamber at time 30 minutes, yielding a final concentration of 10 uM. Next, either shear stress of 10 dyne/cm^2 or a final concentration of 1 U/ml of thrombin was applied at time 60 minutes, and experiments were run for another two hours. In the corresponding control experiments, no shear or thrombin was applied at time 60 minutes.

3.11.7 Increasing NO concentration by application of 500 uM SNAP to cell monolayers

SNAP is soluble in DMSO (57.5 mg/ml) and in water (2.1 mg/ml). The half life of SNAP in aqueous solution is 5 hours. Therefore, SNAP has to be prepared fresh right before the experiments. In this study, SNAP was prepared in two ways: dissolved first in DMSO followed by dilution with experimental media or dissolved directly in experimental media. 1 mg SNAP was dissolved in 100 ul DMSO and further diluted with 1.4 ml of experimental media. 3 ml experimental media was used at the beginning of the experiments and 10 cmH_2O hydrostatic pressure was applied. At time 60 minutes, 0.6 ml of stock solution was added to the luminal side of the chamber, yielding a final concentration of 500 uM. Experiments were conducted for another two hours. In the control experiment, 100 ul DMSO was diluted with 1.4 ml experimental media, 0.6 ml of which was added to the luminal chamber. When SNAP was dissolved directly in experimental media, at time 60 minutes 2 ml of 1 mM SNAP was added to the luminal chamber with 2 ml of experimental media, giving a final concentration of 500 uM SNAP.

3.11.8 Reducing NO concentration by application of L-NMMA to cell monolayers

L-NMMA came in a 5 mg bottle and was reconstituted with 5 ml MEM-1% BSA. 100 ul was then diluted into 4 ml MEM-1% BSA solution, yielding a final concentration of 100 uM. L-NMMA was incubated with cell monolayers at the beginning of the experiment at time zero. Then shear stress of 10 dyne/cm^2 was initiated at time 60 minutes and the L_P experiment was conducted for another two hours.

3.12 Data Presentation and Statistical Analysis

A 1-hour period was allowed for a stable baseline to be established before further intervention. Five-minute Jv/A averages were calculated, normalized in relation to the established baseline (values at 55 minutes), and presented as mean ± SEM (standard error of the mean). Significant differences between group means were analyzed by a two-way (time and treatment) repeated measurement ANOVA using Statistical Analysis Software version 8.0 (SAS).

Chapter 4

Results

4.1 In Vitro Study of Startling's Law

4.1.1 Effect of changing osmotic pressure differential on volumetric flow rate

Figure **4-1** shows the time course of changing the luminal BSA concentration from 1% to 5.5%. Upon application of a hydrostatic pressure gradient of 10 cm H_2O at time 0, a characteristic time-dependent decrease in *Jv* occurred that reached a steady state within an hour. This response, termed the "sealing effect", was previously reported by Sill *et al*. [8]. The value of *Jv* at 55 minutes was chosen as the baseline, and other *Jv* data was normalized by this value to facilitate comparisons among different monolayers. The abluminal concentration was kept at 1% BSA throughout the experiment. For nearly a 10-minute period after the change of luminal concentration at 60 minutes, transmural flow was not detectable, but there was no reversal of flow either. Then the bubble tracker began to record positive flow again at about 70 minutes.

The osmotic pressure of BSA solutions (π in cm H_2O) can be determined from the BSA concentration (C in g/dL) using, $\pi = 3.305\ C + 0.136\ C^2 + 0.0084\ C^3$ [66]. If we use the BSA concentrations in the luminal chamber and abluminal compartment for determining the osmotic pressure differential in Starling's law (Eq. **2.2**), we estimate that π (5.5%) – π (1%) = 20.3 cm H_2O. For a reasonable value of the reflection coefficient,

say $\sigma > 0.7$ (refer to Discussion 5.1), the osmotic driving force is expected to be > 14.2 cm H_2O and readsorption should occur when the hydrostatic pressure differential is 10 cm H_2O. The absence of adsorption in the steady state suggests that the global BSA concentrations do not determine the osmotic pressure differential in Starling's law.

Similar experiments were conducted at 5 cm H_2O and 20 cm H_2O and similar patterns were observed. Steady *Jv* values before and after changing the osmotic pressure at 5 cm H_2O, 10 cmH_2O, and 20 cmH_2O are shown on Figure **4-2**. A decrease in steady state volume flux associated with the increased osmotic pressure in the luminal chamber was clearly observed. But once again, there was no evidence of reabsorption (negative flow) at any time during these experiments even in the case of 5 cm H_2O hydrostatic pressure differential.

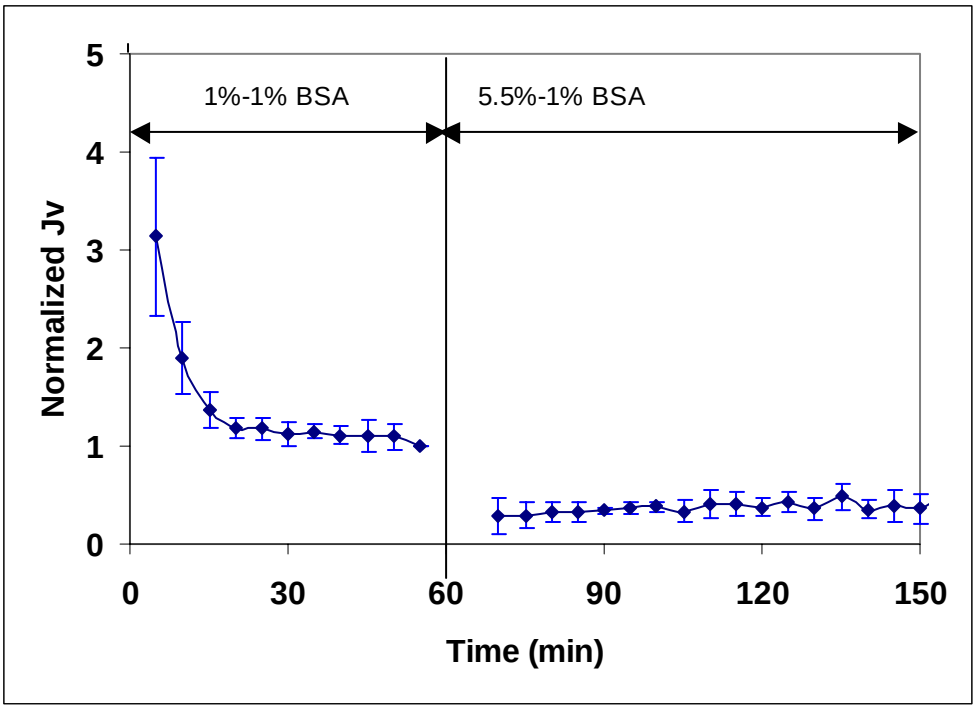

Figure **4-1**: Effect of osmotic pressure on volumetric flow rate at 10 cm H_2O positive pressure differential.

BAECs were seeded on Transwell filter. The luminal concentration of albumin was changed from 1% to 5.5% at time 60 minutes. The abluminal concentration of albumin was maintained at 1%. The baseline Jv/A at 55 minutes was 2.38 ± 0.33 (SEM) x 10^{-6} cm/s·cm H_2O (n=5).

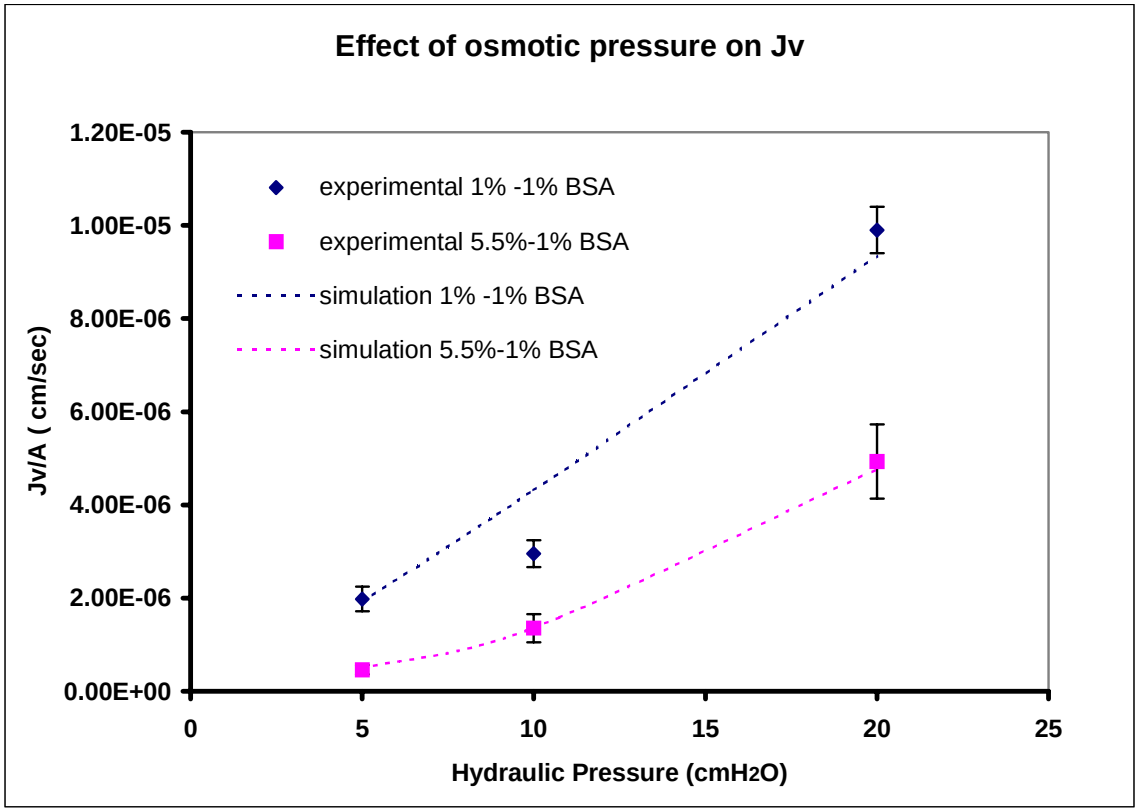

Figure **4-2**: The steady state reduction of volume flux by osmotic pressure at different positive pressure differentials.

BAECs were seeded on Transwell filter. At 5 cm H_2O, volume flux was reduced from $1.98 \pm 0.27 \times 10^{-6}$ cm/s (n=9) at 1% - 1% to $0.46 \pm 0.10 \times 10^{-7}$ cm/s (n=9) at 5.5% - 1%. At 10 cm H_2O, volume flux was reduced from $2.96 \pm 0.29 \times 10^{-6}$ cm/s (n=10) at 1% - 1% to $1.35 \pm 0.3 \times 10^{-7}$ cm/s (n=10) at 5.5% - 1%. At 20 cm H_2O, volume flux was reduced from $9.9 \pm 0.5 \times 10^{-6}$ cm/s (n=9) at 1% - 1% to $4.9 \pm 0.80 \times 10^{-6}$ cm/s (n=9) at 5.5% - 1%.

4.1.2 Effects of changing hydrostatic pressure differential on volumetric flow rate

Because it is difficult to introduce a sudden change in osmotic pressure across the endothelial layer, as we attempted in the experiments summarized in Figure **4-1** and

Figure **4-2**. We introduced a rapid change in hydrostatic pressure in the next series of experiments. With 5.5% BSA in the luminal compartment and 1% BSA in the abluminal compartment, the hydrostatic pressure differential was quickly changed from 20 cm H_2O to 5 cm H_2O. In this case, a transient reversal of flow was observed (Figure **4-3**). The magnitude of the peak reverse flow was much higher than expected for the overall Starling driving force, but it decayed quickly as indicated in Figure **4-4**. There was a period of nearly 20 minutes after decay of the reversal flow during which transmural flow could not be detected in either direction (Figure **4-3**). After that period, positive flow resumed and approached a steady state level.

In the control experiment with1% BSA on both sides of the endothelial layer, where the global osmotic pressure difference was zero throughout the experiment, the sudden change of hydrostatic pressure from 20 cm H_2O to 5 cm H_2O did not cause readsorption (data not shown), indicating that the transient readsorption was due to the osmotic pressure differential, not an artifact such as instantaneous volume change due to the deformation of the filter membrane after the pressure change or significant fluid accumulation under the monolayer when the pressure differential was reversed.

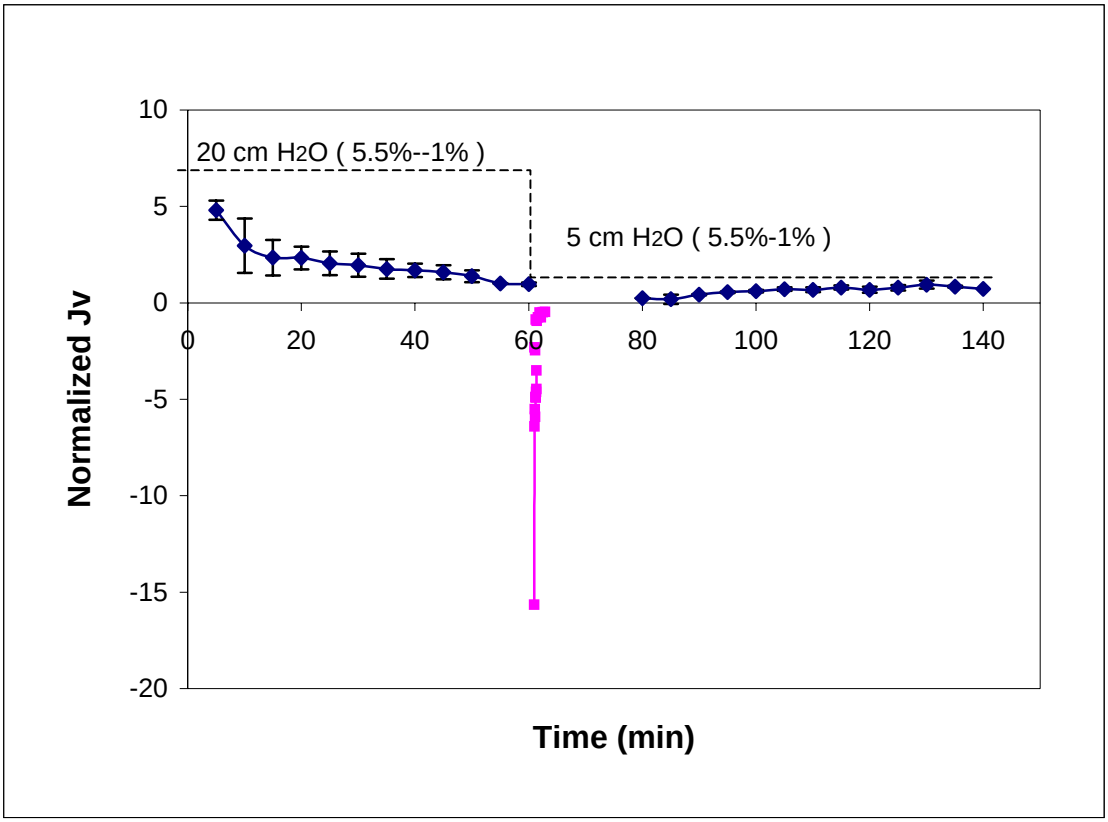

Figure **4-3**: Transient reversal of volumetric flow rate after a sudden reduction of hydrostatic pressure differential from 20 cm H_2O to 5 cm H_2O.

BAECs were seeded on Transwell filters. The luminal and abluminal albumin concentrations (5.5% - 1%) were not changed. The transient reversal phase is enlarged in Figure **4-4**. The baseline Jv/A was 3.11 ± 0.07 x 10^{-6} cm/s (n=4).

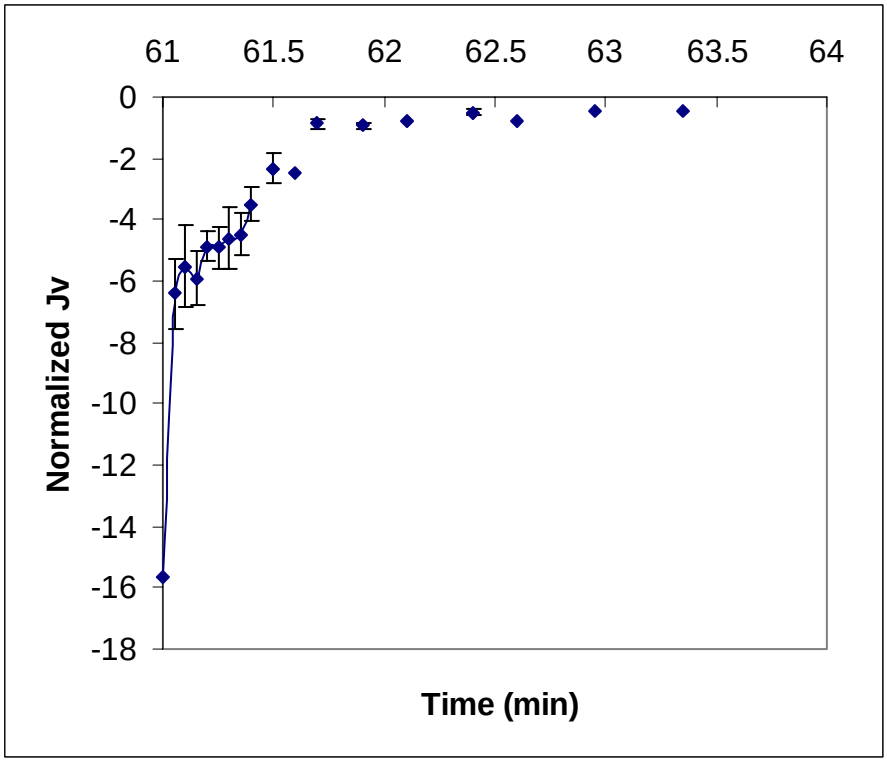

Figure **4-4**: Transient reversal of volumetric flow rate – enlargement of Figure **4-3** .

4.1.3 Effect of negative pressure differential on hydraulic conductivity

The high reverse flow recorded in the experiments of Figure **4-3** suggested that the hydraulic conductivity of the vitro monolayer might be asymmetric, with higher values for flow in the direction of reabsorption. To test this, we placed 1% BSA in both the luminal and abluminal compartments to minimize the osmotic pressure effect so that the hydraulic conductivity could be determined from the classical Starling's law (Eq. **2.2**) as follows:

$$L_P = \frac{Jv}{A \cdot \Delta P} \qquad \textbf{4.1}$$

In view of the more general modified Starling law (Eq. **2.4**) Eq. **4.1** must be considered an approximation. However, using reasonable values of the parameters σ and P_d (discussed in a subsequent section), the approximation underestimates L_P by only 16% at 10 cm H_2O. The L_P values calculated using Eq. **4.1** are listed in Table **4-1**.

The hydraulic conductivity for reverse flow was much higher (about 100 fold) than for forward flow, indicating a highly asymmetric transport barrier. Figure **4-5** shows a typical time course of Jv when pressure differential was alternated. When pressure differential was changed from 10 cm H_2O to –2 cm H_2O, a high reverse flow was observed that kept increasing during the first 5 min and reached a plateau at 10 min. Return to a positive pressure differential (10 cm H_2O) was followed by a "sealing" period similar to the one following the initial exposure to 10 cm H_2O pressure differential. Recovery ($L_{p\text{final}} / L_{p\text{initial}}$) from –2 cm H_2O differential pressure was 120% after return to +10 cm H_2O differential pressure, suggesting that the cell monolayer was not altered very

much by the reverse flow period. However, at higher reverse pressures of –4 cm H_2O and -10 cmH_2O, recovery data indicated somewhat greater alteration of the monolayer.

Table **4-1**: **Asymmetric nature of the endothelial transport barrier**

Pressure (cm H_2O)	L_P (cm/s•cm H_2O)	L_P Normalized with 10 cm H_2O value	Recovery L_{Pfinal} / $L_{Pinitial}$
-10	$2.53 \pm 0.39 \times 10^{-5}$ (n=3)	85.5 ± 13.2	200%
-4	$5.32 \pm 0.12 \times 10^{-5}$ (n=3)	178 ± 4.1	150%
-2	$1.47 \pm 0.16 \times 10^{-5}$ (n=9)	49.7 ± 5.4	120%
10	$2.96 \pm 0.29 \times 10^{-7}$ (n=10)	1 ± 0.09	N/A

Note: $L_{Pinitial}$ is the L_p value at time 55 minutes while L_{Pfinal} is the L_p value at time 135 minutes after the re-establishment of the baseline (Figure **4-5**)

4.1.4 Visualization of monolayer

Selected monolayers stained with calcein AM were visualized under a microscope at 100×. There were no apparent areas of endothelial denudation or cell death after experimental treatments including reverse flow experiments.

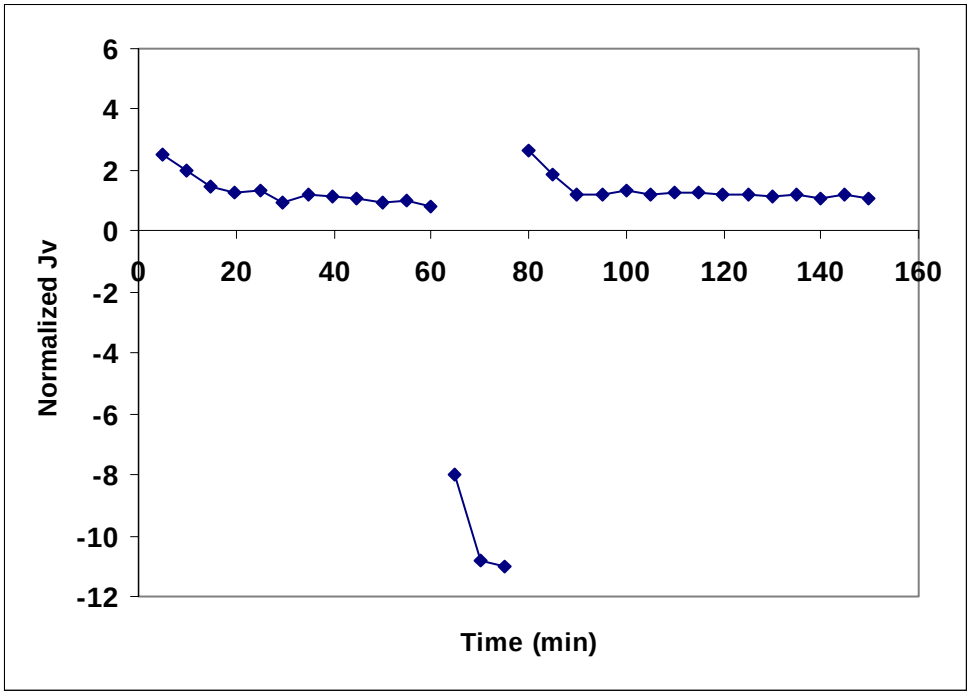

Figure **4-5**: A typical time course of *Jv* at alternately positive and negative pressure differentials

Pressure differential was 10 cm H_2O for first hour and a negative pressure differential (-2 cm H_2O) was then applied for another 20 minutes before it was returned to 10 cm H_2O

4.2 Effect of Shear Stress on HUVEC L_P

Both steady and oscillatory shear stresses were applied to HUVEC monolayers to investigate their effects on endothelial Lp. 20, 10, and 5 dyne/cm^2 were used for the study of steady shear stress. 0 ± 20 dyne/cm^2 was used for the study of pure oscillatory shear stress, and 10 ± 5, 10 ± 10, and 10 ± 15 dyne/cm^2 (with shear reversal) were used for the study of steady and oscillatory shear stresses simultaneously.

4.2.1 Effect of steady shear stress on HUVEC L_P

Figures **4-6** to Figure **4-8** depict the effect of 20, 10, and 5 dyne/cm^2 shear stress on HUVEC Lp, respectively. In all cases, steady shear stress induced a transient increase of L_P, followed by a decay back to normal compared to their control experiments (10 cmH_2O hydrostatic pressure differential and no shear). The magnitudes of steady shear stress affected the maximum increase and the duration of the transient period. Specifically, 20 dyne/cm^2 shear stress elevated L_P 1.7 fold at time 75 minutes, and the duration of this transient period was about 80 minutes (from 70 minutes to 150 minutes), whereas 10 dyne/cm^2 shear stress elevated baselines up to 2.35 folds (a magnitude slightly higher than that of 20 dyne/cm^2), but the transient period lasted for only 45 minutes (from 65 minutes to 105 minutes). 5 dyne/cm^2 shear stress also elicited up to a 1.7 fold transient increase that lasted for only 15 minutes (from 105 minutes to 120 minutes). Statistically there was no significant difference between the maximum elevation at 20, 10, and 5 dyne/cm^2 (*t-test*, P>0.1).

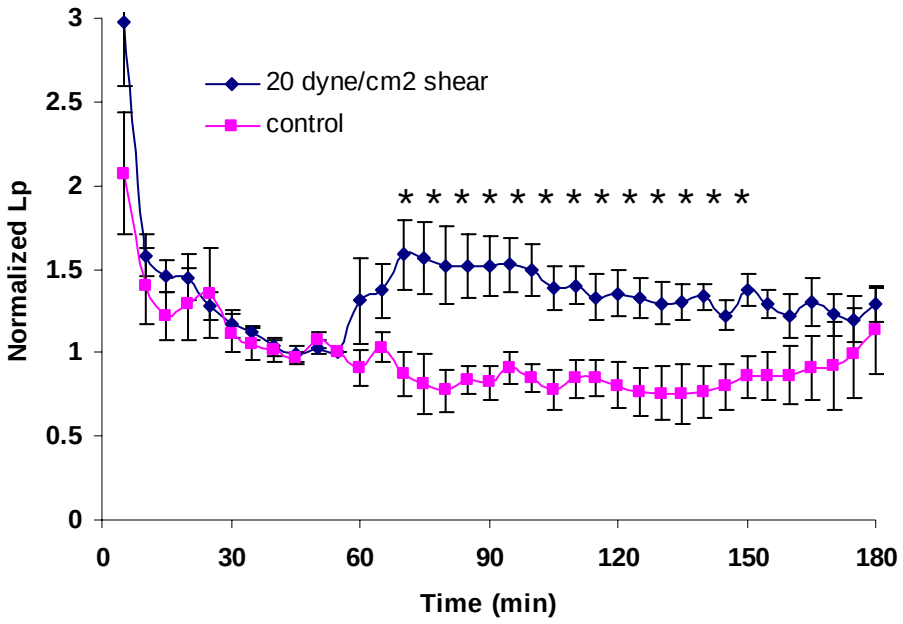

Figure **4-6**: Effect of 20 dyne/cm^2 shear stress on HUVEC L_P

10 cm H_2O hydrostatic pressure was applied at time 0 and 20 dyne/cm^2 shear stress was applied at time 60 minutes. Shear stress elevated the baseline by 1.7 fold and kept for about 80 minutes before it returned to normal. Baseline L_P for shear was 3.03 ± 0.62 $\times 10^{-7}$ cm/sec/cmH_2O (n=8), and Baseline L_P for control was 2.92 ± 1.24 $\times 10^{-7}$ cm/sec/cmH_2O (n=4). Data was presented as mean ± SEM. * denoted the significant difference between shear and control experiments ($P<0.05$)

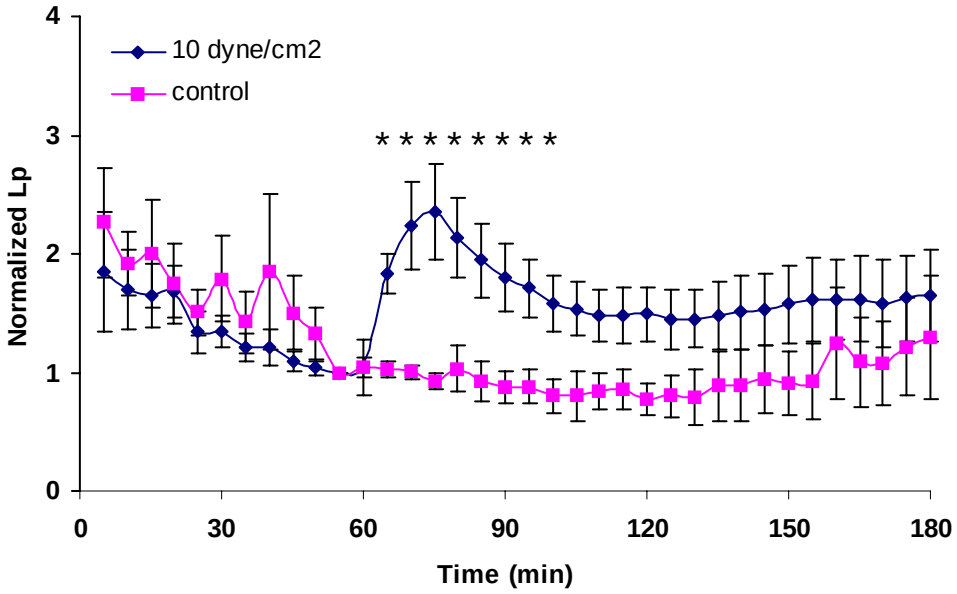

Figure **4-7**: Effect of shear stress of 10 dyne/cm^2 on HUVEC L_P

10 cm H_2O hydrostatic pressure was applied at time 0 and 10 dyne/cm^2 shear stress was on at time 60 minutes. Shear stress elevated the baseline by 2.35 fold at time 75 minutes and kept for about 40 minutes before it returned to normal. Baseline L_P for shear was 4.88 ± 0.61 $\times 10^{-7}$ cm/sec/cmH_2O (n=6), and Baseline L_P for control was 2.33 ± 0.85 $\times 10^{-7}$ cm/sec/cmH_2O (n=3). Data was presented as mean ± SEM. * denoted the significant difference between shear and control experiments ($P<0.05$)

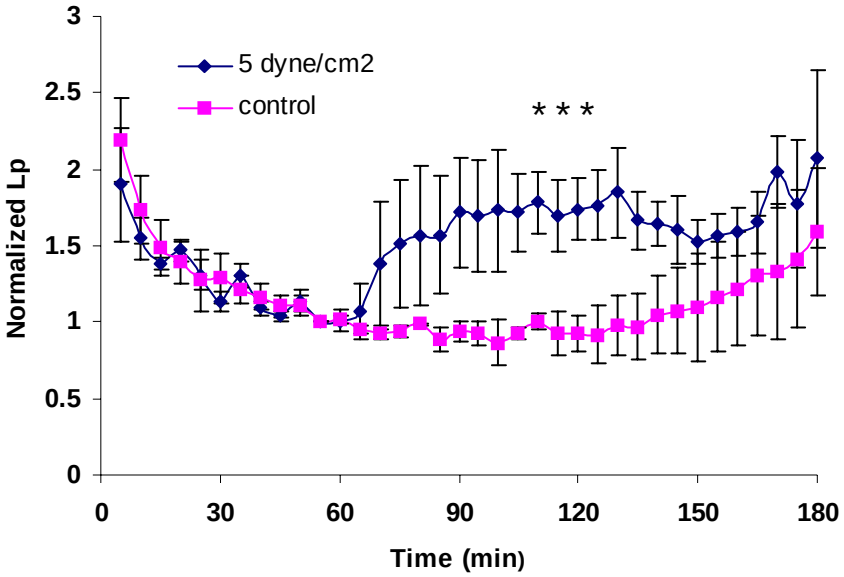

Figure **4-8**: Effect of shear stress of 5 dyne/cm^2 on HUVEC L_P

10 cm H_2O hydrostatic pressure was applied at time 0, and 5 dyne/cm^2 shear stress was applied at time 60 minutes. Shear stress elevated the baseline by 1.7 fold and kept for about 15 minutes before it returned to normal. Baselines for shear were $3.35 \pm 0.90 \times 10^{-7}$ cm/sec/cmH_2O (n=3), and Baselines for control were $3.13 \pm 0.16 \times 10^{-7}$ cm/sec/cmH_2O (n=3). Data was presented as mean ± SEM. * denoted the significant difference between shear and control experiments ($P<0.05$)

4.2.2 Effect of oscillatory shear stress on HUVEC L_P

The effect of pure oscillatory shear stress on HUVEC L_P is shown in Figure **4-9**. Shear stress of 0 ± 20 dyne/cm^2 was applied at time 60 minutes, and no effect on Lp compared to the control (no shear) was observed during the two hour exposure of oscillatory shear stress, implying that oscillatory shear stress and steady shear stress elicited different effects on HUVEC L_P.

To investigate steady and oscillatory shear stresses simultaneously, a constant steady shear stress of 10 dyne/cm^2 was superimposed by an oscillatory shear stress of 5, 10, and 15 dyne/cm^2 amplitude, respectively. It should be noted that there was a shear reversal when the oscillatory shear amplitude was 15 dyne/cm^2. The results are shown in Figure **4-10**. 10 dyne/cm^2 shear stress induced a more than 2 fold increase in Lp, consistent with previous results in Figure **4-7**. Superposition of oscillatory shear stress on this steady shear stress suppressed the transient effect. The L_P responses to 10 ± 15 dyne/cm^2, 10 ± 10 dyne/cm^2, 10 ± 5 dyne/cm^2 were not statistically different from the control (no shear), but were statistically different from the corresponding steady shear stress case. In addition, there was no statistical difference between 10 ± 5 dyne/cm^2 and 10 ± 15 dyne/cm^2, suggesting that oscillatory components, not the direction change, determined the effect of oscillatory shear. As low as 5 dyne/cm^2 oscillatory shear stress amplitude was enough to block the effect of a steady shear stress component of 10 dyne/cm^2.

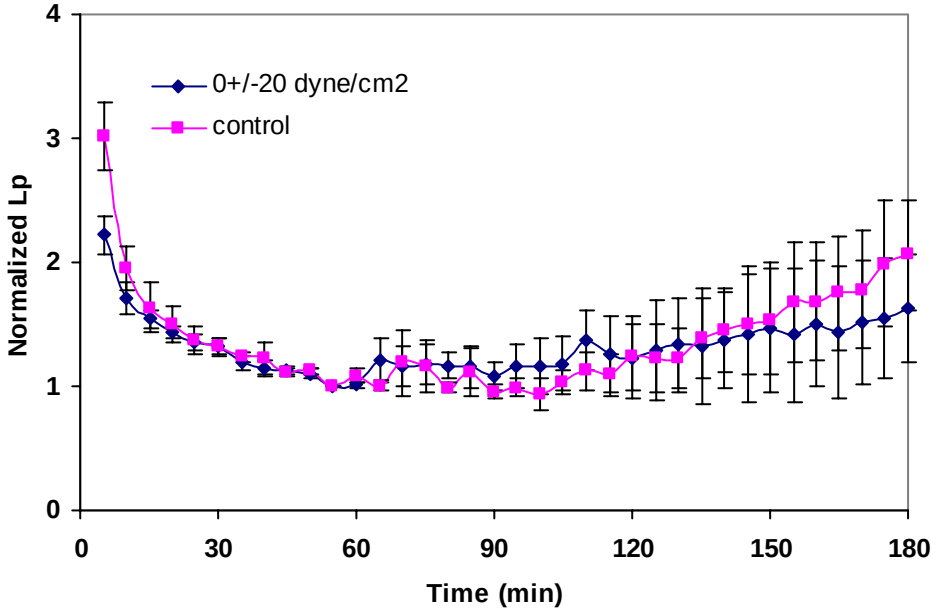

Figure **4-9**: Effect of pure oscillatory shear stress of 0 ± 20 dyne/cm^2 on HUVEC L_P

10 cm H_2O hydrostatic pressure was applied at time 0 for both shear and control experiments and 0 ± 20 dyne/cm^2 shear stress was set at time 60 minutes for shear experiment. Oscillatory shear stress had no effect on HUVEC L_P. Baselines for shear stress at 0 ± 20 dyne/cm^2 were 2.97 ± 0.66 $\times 10^{-7}$ cm/sec/cmH_2O (n=5), and the corresponding baseline for control is 3.98 ± 1.8 $\times 10^{-7}$ cm/sec/cmH_2O (n=3). Data was presented as mean ± SEM. There was no significant difference between shear and control experiments

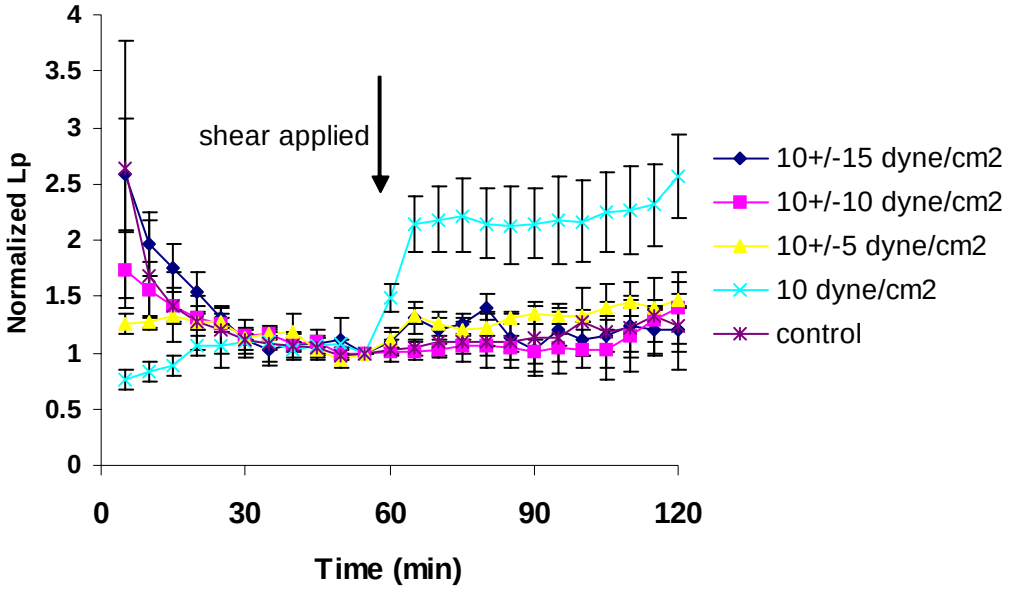

Figure **4-10**: Effect of oscillatory components superposed on steady shear stress on HUVEC L_p

After the establish of baseline, steady shear stress 10 dyne/cm^2 shear stress and a superimposed oscillatory shear stress (10 ± 10 dyne/cm^2, and 10 ± 5 dyne/cm^2) with an average of 10 dyne/cm2 shear stress was applied and the volume flux was monitored for another hour. The Baseline for 10 dyne/cm^2 is 4.03 ± 0.63 × 10^{-7} cm/sec/cmH_2O (n=4), for 10 ± 5 is 4.20 ± 0.35 × 10^{-7} cm/sec(n=4) , 10 ± 10 is 4.25 ± 0.87× 10^{-7} cm/sec/cmH_2O (n=5) 10 ± 15 dyne/cm^2 was 2.97 ± 1.14 × 10^{-7} cm/sec/cmH_2O (n=4). The control experiment baseline is 4.31 ± 1.68 × 10^{-7} cm/sec/cmH_2O (n=3).

4.3 Signal Transduction Pathways

4.3.1 Effect of calcium pathway in regulation of HUVEC L_P

4.3.1.1 Effect of thrombin, a calcium agonist, on HUVEC L_P

Thrombin is a known agonist for EC transport that is mediated by the calcium pathway. Figure **4-11** illustrates the thrombin effect on HUVEC hydraulic conductivity. At time 60 minutes thrombin was added to a final concentration of 1 U/ml, and a transient increase in L_P up to 2.5 fold occurred quickly at 65 minutes. L_P decayed rapidly within 20 minutes and then returned to normal baseline after 80 minutes. There was a significant difference between thrombin and control (no thrombin) from time 65 minutes to time 75 minutes ($P<0.05$). This response was similar to that of steady shear stress, but at a much more acute rate. 2 U/ml thrombin irreversibly elevated L_P and the baselines kept increasing, suggesting that cell monolayers suffered some permanent damage by the high dose of thrombin and that the integrity of the cell monolayers was compromised. Therefore 1 U/ml thrombin was applied to cell monolayers for the remaining experiments.

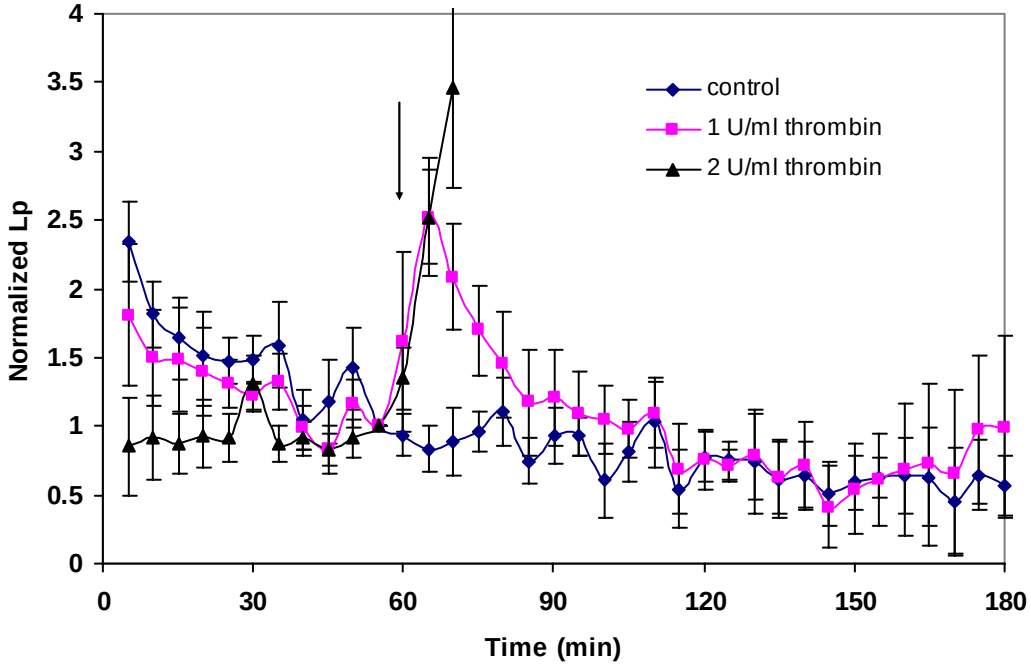

Figure **4-11**: Effects of thrombin on HUVEC L_P

10 cm H_2O hydrostatic pressure was applied at the beginning. At time 60 minutes, concentrated thrombin solution was added to yield a final concentration of 1 U/ml thrombin. 1 U/ml thrombin transiently increased L_P and returned to normal in 30 minutes. The L_P at time 55 minutes for 1 U/ml thrombin was 2.51 ± 0.67 $\times 10^{-7}$ cm/sec/cmH_2O (n=4), and control was 2.48 ± 0.28 $\times 10^{-7}$ cm/sec/cmH_2O (n=4).There were significant difference between 1 U/ml shear and control from 65 minutes to 75 minutes ($P<0.05$).

4.3.1.2 Effect of BAPTA-AM on thrombin response

BAPTA, a selective calcium chelator (K_d = 700 nM) is widely used in the study of the calcium pathway. BAPTA-AM is an ester form of BAPTA, and due to its AM group, it can be transported through the cell membrane and is degraded to BAPTA in the cytosol. Therefore, BAPTA-AM can chelate intracellular calcium concentration, and is widely used to study the effect of intracellular calcium.

Figure **4-12** depicts the effect of 10 uM BAPTA-AM on the thrombin response. 10 uM BAPTA-AM was applied to cell monolayers at 30 minutes, resulting in an immediate decrease in volume flux (Jv/A). Addition of thrombin (1 U/ml final concentration) at 60 minutes did not induce any effect until 30 minutes later, whereas in the absence of 10 uM BAPTA-AM, 1 U/ml thrombin increased volume flux immediately (control experiment with 1 U/ml thrombin). The volume flux for the experiments in the presence of both 10 uM BAPTA-AM and 1 U/ml thrombin started to increase after 90 minutes. This increase is a result of thrombin exposure since in the control experiment with only 10 uM BAPTA-AM, the volume flux kept a fairly constant value. Therefore, BAPTA-AM delayed the thrombin response, indicating that calcium pathway was involved in the regulation of hydraulic conductivity.

It should also be noted that in this thrombin experiment, the increased baseline stimulated by thrombin failed to return to normal as illustrated previously in Figure **4-11.** This might reflect the variation in lots of thrombin. According to the manufacturer, 1 U/ml thrombin was equivalent to 2000-3000 NIH U/ml. The NIH unit was obtained by

direct comparison to a NIH Thrombin Reference Standard, lot J., The thrombin response shown in Figure **4-12** seemed to be in between the thrombin responses at 1 U/ml and 2 U/ml in Figure **4-11**.

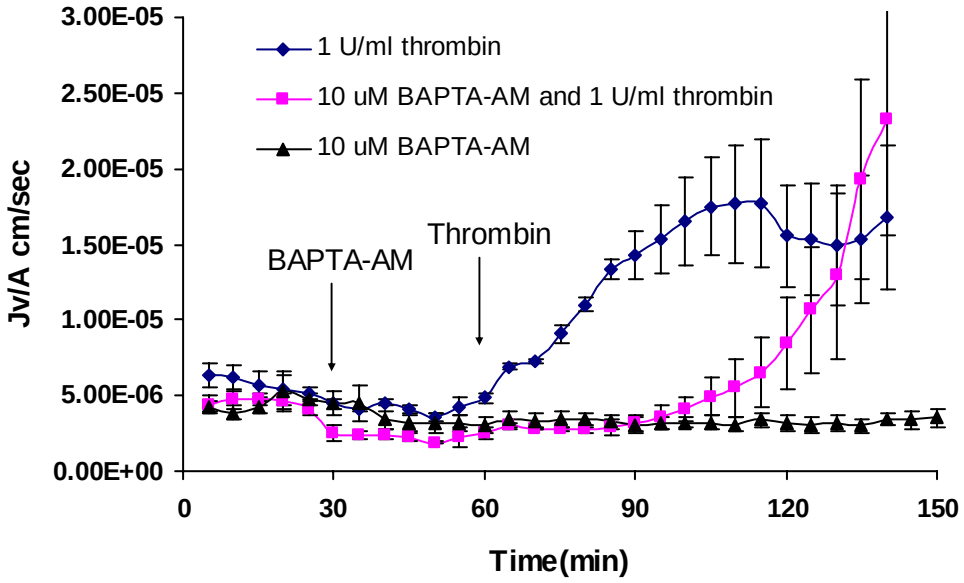

Figure **4-12**: The inhibition effect of BAPTA-AM on HUVEC thrombin response

10 uM BAPTA was added at time 30 minutes in the BAPTA and thrombin experiment, and 1 U/ml thrombin was added at time 60 minutes in both experiments. Application of 10 uM BAPTA reduced the baselines from 4.15 $\times 10^{-6}$ cm/sec to 2.83 $\times 10^{-6}$ cm/sec. Addition of thrombin caused an immediate increase of baseline when BATPA-AM was absent. For the experiments with 10 uM BAPTA-AM, this process was significantly delayed.

.

4.3.1.3 Effect of BAPTA-AM on shear response

The effect of BAPTA-AM on the shear response of HUVEC L_P is depicted in Figure **4-13**. 10 uM BAPTA-AM was added at 30 minutes, resulting in a reduction of baselines as we observed before. At time 60 minutes, shear stress of 10 dyne/cm^2 was applied, and a typical shear response was observed in the presence and absence of BAPTA-AM (control experiment with 10 dyne/cm^2 shear stress only). Surprisingly, the depletion of intracellular calcium failed to block the shear response, providing strong evidence that the calcium pathway is not involved in the shear response.

BAPTA-AM alone caused a reduction in L_P. Due to the "sealing effect", baselines naturally decreased by 20% from time 25 minutes to 35 minutes, whereas they dropped by 40% in the presence of BAPTA-AM in the same period (Figure **4-14).** This difference was statistically significant (P= 0.04).

In all BAPTA-AM experiments, only a tiny amount of DMSO was used to dissolve BAPTA-AM and the final concentration of DMSO was negligible (0.13 ul in 4 ml experimental media). Therefore DMSO did not exert any effect on HUVEC L_p.

In summary, the calcium pathway is involved in the regulation of cell permeability, as evidenced by the observations that BAPTA-AM delayed the thrombin response and that BAPTA-AM decreased L_P. However, no effect of BAPTA-AM on the shear response indicates that the shear response is independent of calcium pathway.

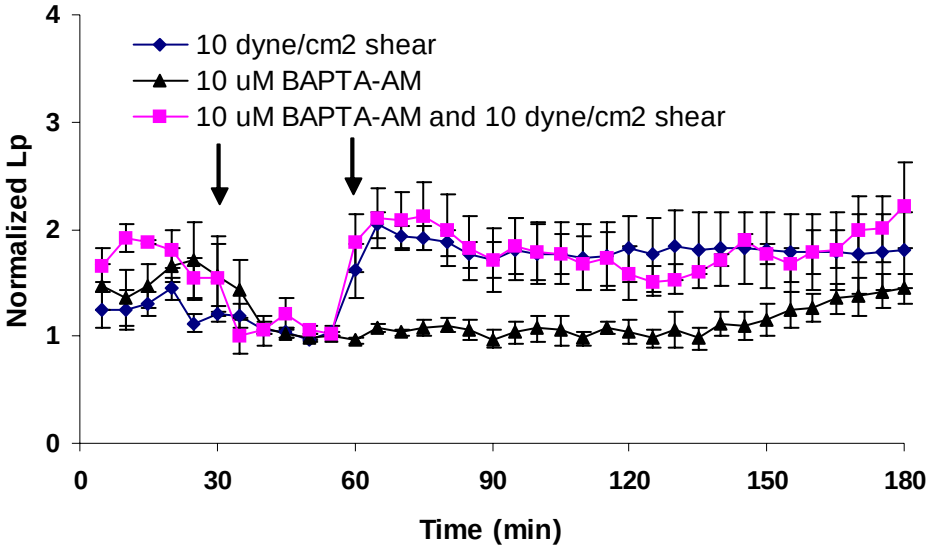

Figure **4-13**: BATPA-AM has no effect on shear response of HUVEC.

10 mM BAPTA-AM was administered at time 30 minutes, causing a reduction at the baseline. Shear was turned on at time 60 minutes for both control and BAPTA-AM experiments. No effect was observed for the BATPA-AM. The baseline for 10 dyne/cm^2 was 4.88 ± 1.08 × 10^{-7} cm/sec/cmH_2O (n=4) and the 10 mM BAPTA –AM and 10 dyne/cm^2 baseline were 2.48 ± 0.25 × 10^{-7} cm/sec/cmH_2O (n=4), and the baselines for 10 mM BAPTA-AM alone were 3.17 ± 0.56 × 10^{-7} cm/sec/cmH_2O (n=5).

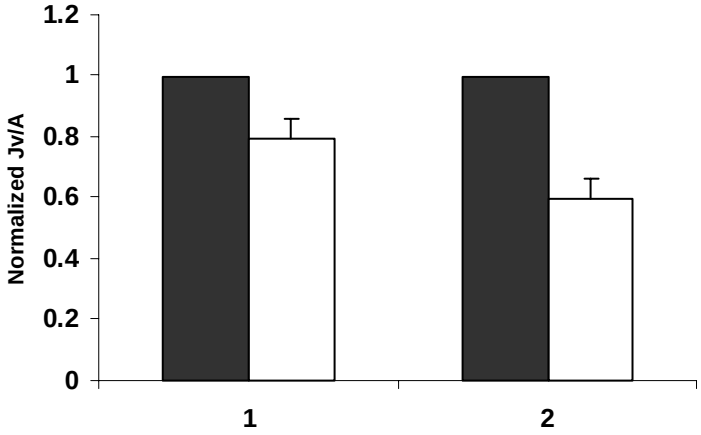

Figure **4-14**: Reduction of HUVEC baselines by BAPTA-AM

In the case 1: no BAPTA-AM was added during the experiment, In the case 2: 10 uM BATPA-AM was added at time 30 minutes. All the Jv/A values were normalized to the Jv/A values at time 25 minutes. The black bar was normalized Jv/A at time 25 minutes and hence 1. The open bar was normalized Jv/A values at time 35 minutes. Jv/A values at 25 minutes was $5.16 \pm 0.43 \times 10^{-6}$ cm/sec for the control (n=3), and $4.06 \pm 0.66 \times 10^{-6}$ cm/sec for the experiment with 10 uM BAPTA-AM (n=5)

4.3.2 NO signal transduction pathway

4.3.2.1 Effect of shear stress on NO production

As shown in Figure **4-15**, all shear stress patterns stimulated nitrite production in HUVEC. In stationary cultures, cells produced nitrite at a much lower lever, around 10 nmol/mg protein. Steady shear of 20 dyne/cm^2 and 10 dyne/cm^2 elevated nitrite concentration to 61 nmol/mg protein and 38 nmol/mg protein, respectively, from a base level of 17 nmol/mg protein at time 180 minutes. Oscillatory shear stress of 10 ±15 dyne/cm^2 increased nitrite concentration higher than steady shear of 10 dyne/cm^2 did, and the elevated concentration (56 nmol/mg protein)was comparable to that of 20 dyne/cm^2 (61 nmol/mg protein) Statistically, there was no significant difference between these shear stresses in terms of nitrite concentration, although all of them were significantly different from the control experiment after 120 minutes ($P<0.05$). It should also be noted that the production rate of nitrite (the slope of concentration) was higher at the onset of the shear stress and lower at later times, which was consistent with the report by Kuchan *et al.* [67].

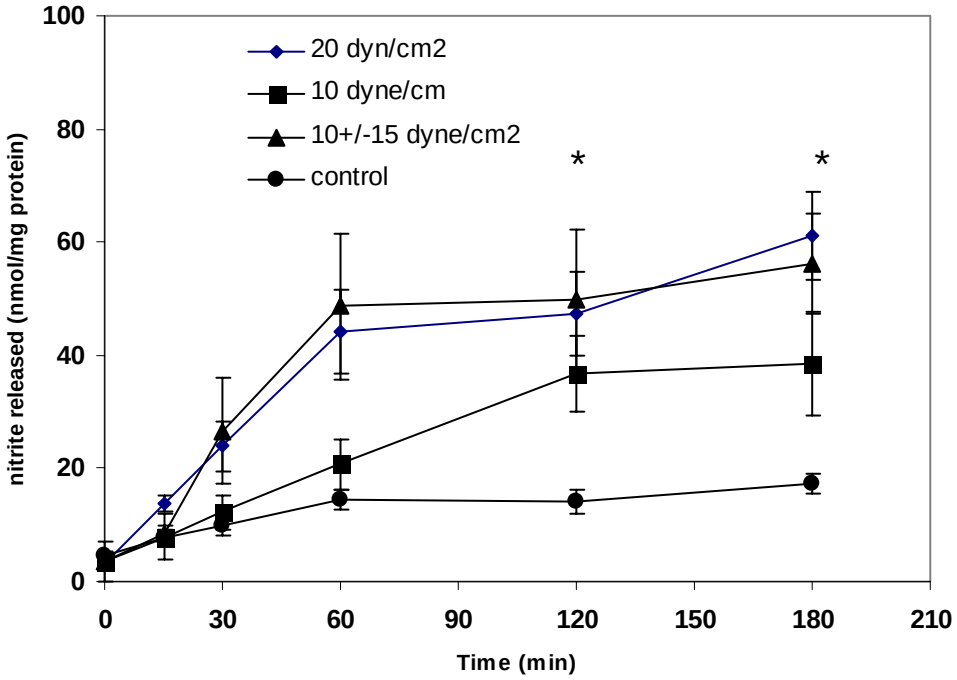

Figure **4-15**: NO production at different level of shear stress

Steady and oscillatory shear stress elevated the production of nitrite (nitrite concentration was used as an indicator for NO concentration), N=8 for 20 dyne/cm^2, n=7 for 10 dyne/cm^2, n=10 for 10 ± 15 dyne/cm^2, and n=8 for control experiment. * denoted that at these values (for all cases) were significantly different from the corresponding control values ($P<0.05$)

4.3.2.2 Effect of increasing NO level by adding SNAP on HUVEC L_P

SNAP is an exogenous NO donor, and the addition of SNAP increases the NO concentration. In general, SNAP is dissolved using DMSO as a vehicle due to its high solubility in DMSO. Figure **4-16**A shows the effect of SNAP on L_P using DMSO as a solvent. 500 uM SNAP increased baselines by 3 fold after two hours. However, the same amount of DMSO that was used to dissolve SNAP could also elicit an increase to the same extent, implying that it was DMSO itself, not SNAP, that caused L_P to be elevated. In order to eliminate the effect of DMSO, SNAP was dissolved directly into experimental media (MEM-1% BSA). SNAP without DMSO appeared to increase L_P slightly, but the increases were not statistically significant at any time point (Figure **4-16**B). As a whole, SNAP had no effect on HUVEC L_P.

(A) SNAP experiments using DMSO as a solvent

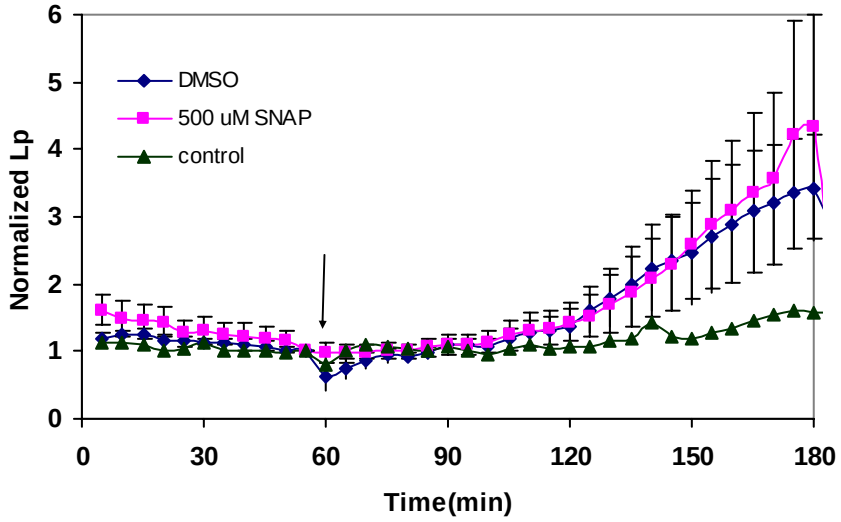

(B) SNAP experiments using water as a solvent

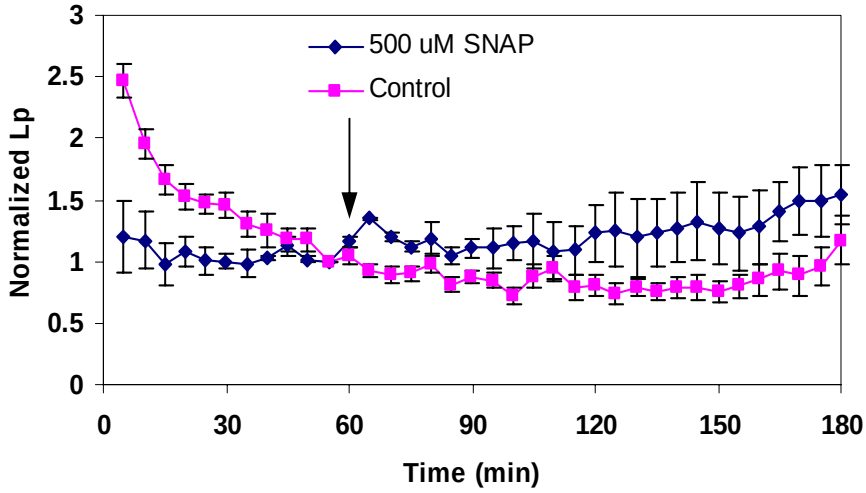

Figure **4-16**: Effect of SNAP on HUVEC L_P

(A) SNAP increased Lp, After the establishment of baseline L_P, SNAP was added at time 60 minute. 500 uM SNAP baseline 4.86 ± 1.61 $\times 10^{-7}$ cm/sec/cmH_2O (n=6), The baselines for DMSO are 4.67 ± 0.51 $\times 10^{-7}$ cm/sec/cmH_2O (n=4) (B): Baselines for SNAP were 3.25 ± 0.23 $\times 10^{-7}$ cm/sec/cmH_2O (n=3), the control experiments were same as figure. In both A and B cases, there is no significant difference between SNAP and control experiments

4.3.2.3 Effect of reducing NO concentration on HUVEC L_P

L-NMMA, a NOS inhibitor, inhibits the generation of NO from arginine. Application of L-NMMA leads to NO concentration reduction, therefore potentially impacting HUVEC Lp.

Figure **4-17A** shows the effect of L-NMMA on the shear response of L_P. Cells were incubated with 100 uM L-NMMA for 60 minutes at 10 cmH_2O hydrostatic pressure before the application of shear stress of 10 dyne/cm^2, allowing sufficient time for L-NMMA to react with cells. In the absence of 100 uM L-NMMA, 10 dyne/cm^2 shear stress elevated L_P by 2 fold, which was similar to the results in Figure **4-7**, while in the presence of 100 uM L-NMMA, shear stress elevated L_P by almost 3 fold, an increase higher than that of steady shear stress alone. However, there was no statistically significant difference between these two treatments (with and without L-NMMA). There was absolutely no inhibition observed during the experiments, suggesting that NO was not functional in HUVEC L_P regulation. Figure **4-17B** illustrates the effect of L-NMMA on HUVEC L_P in the absence of shear stress. Treatment with 100 uM L-NMMA shows no difference from the control.

Although oscillatory and steady shear stress increased NO production significantly, increasing or decreasing of NO concentration using SNAP and L-NMMA showed no effect on L_P, suggesting that the NO pathway was not functioning in HUVEC L_P regulation.

(A) 100 uM L-NMMA has no inhibitory effect on shear response

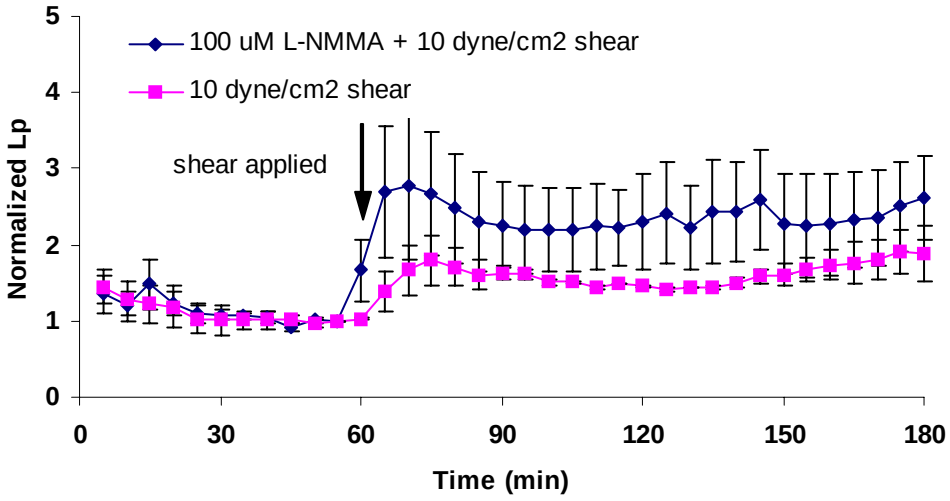

(B) 100 uM L-NMMA has no effect on HUVEC baselines

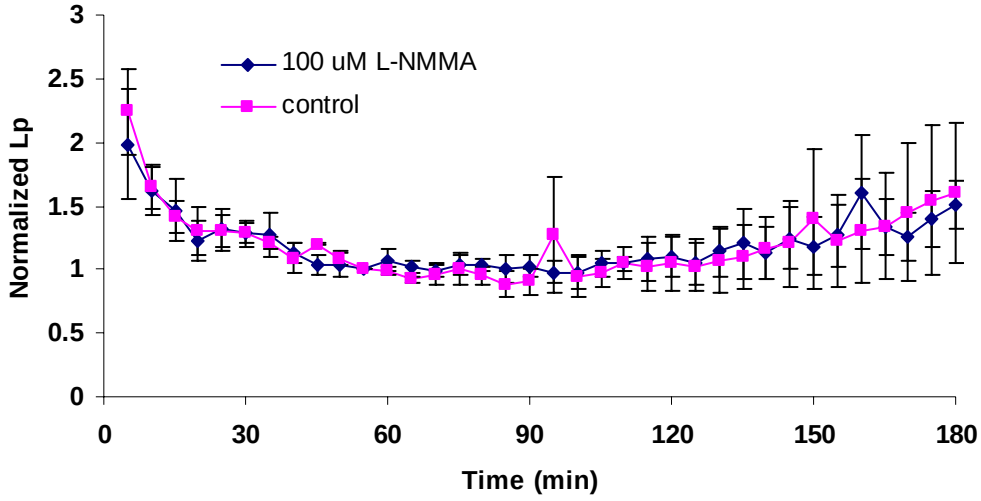

Figure **4-17**: Effects of L-NMMA on HUVEC L_P

(A) Baselines for L-NMMA + shear were 4.20 ± 0.60 × 10^{-7} cm/sec/cmH_2O (n=4), and baselines for shear were 4.36 ± 0.30 × 10^{-7} cm/sec/cmH_2O (n=4), (B) Baselines for L-NMMA were 2.93 ± 0.31 × 10^{-7} cm/sec/cmH_2O (n=3), and baselines for control were 4.14 ± 0.67 × 10^{-7} cm/sec/cmH_2O (n=3). 100 uM L-NMMA was applied at the beginning of the experiments.

4.4 The Role of Occludin in HUVEC L_P Regulation

4.4.1 Determination of occludin molecular weight

The molecular weight (MW) of occludin is determined by its migration relative to that of protein standards with known MWs. The migration of protein standards is plotted against log of MW in Figure **4-18A**, and a quadratic equation was used for curve fitting. Knowing the migration of occludin, its MW was determined by this curve. Occludin appeared as several bands on the gel with migration at 4.1 cm, 4.2 cm, 5 cm, 6.5 cm, 8.9 cm and 10.6 cm (Figure **4-18B**), yielding MWs at 61 kDa, 59 kDa, 50 kDa, 38 kDa, 26kDa, and 21 kDa. Of them, 61 kDa and 59 kDa were predominant and represented two phosphorylation states of occludin: phosphorylated and dephosphorylated, as proven by the fact that addition of alkaline phosphatase (CIP) caused the 61 kDa occludin band to collapse into the 59 kDa band (Figure **4-19D**)**.** The different phosphorylation states of occludin have been observed in BAEC [59], where α and β occludin referred to the nonphosphorylated and phosphorylated states, respectively. The ratio of the amount of β occludin to that of α occludin is defined as phosphorylation ratio, which equals to ratio of peak area shown in Figure **3-8**. The determined molecular weight of occludin as well as its degraded products (MWs of 50 kDa, 38 kDa, 26 kDa, and 21 kDa) confirmed with other reports in HUVEC. For instance, Wachtel [68]reported occludin molecular weight at 61 kD with a degraded product at 50 kDa. Therefore it is very important to promptly treat the samples to avoid proteolysis.

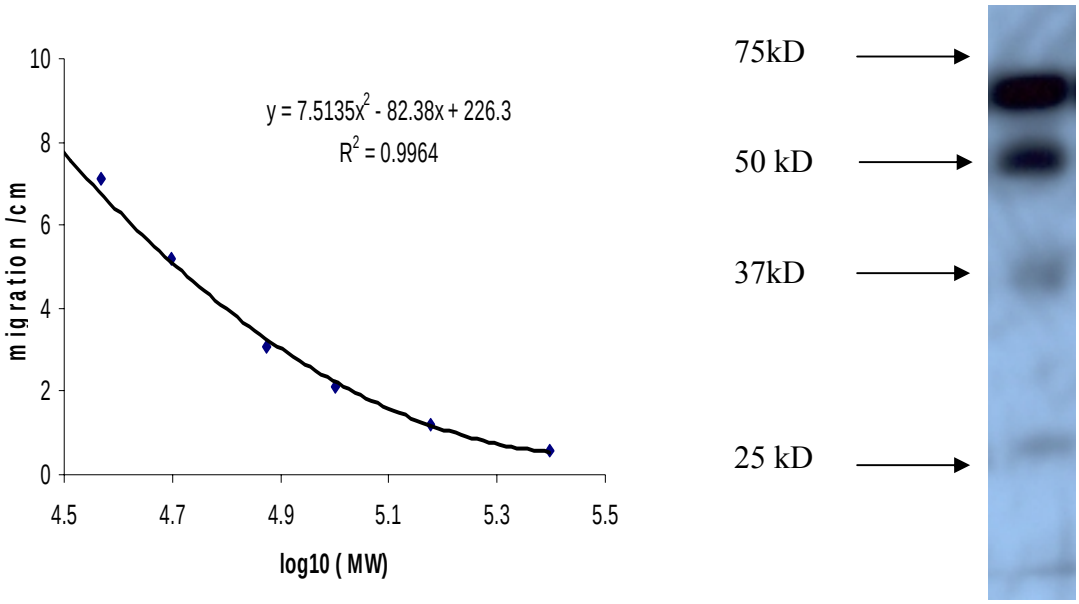

(A) (B)

Figure **4-18**: Determination of occludin molecular weight

Precision molecular weight marker is from Bio-Rad with molecular weights of 25, 37, 50, 75, 100, 150, and 250 kDa (arrows in panel B). The migration of occluding is at 4.1, 4.2, 5, 6.5, 8.9, 10.6 cm, corresponding to molecular weights of 61, 59, 50, 26, and 21 kDa.

4.4.2 Total amount of occludin and phosphorylation state of occludin under different experimental conditions

Figure **4-19** illustrates the time profile of occludin phosphorylation after the application of shear stress of 10 dyne/cm^2 (A), 1 U/ml thrombin (B), and oscillatory shear stress of 10 ± 15 dyne/cm^2 (C). Application of 10 dyne/cm^2 shear stress significantly increased occludin phosphorylation ratio from 1 (control) to 1.85 at 30 minutes ($P<0.01$), and then the ratio returned to 1.3 at 120 minutes (not significantly different from the control; $P=0.13$). The phosphorylation ratio versus time profile showed similarity to the hydraulic conductivity response to shear stress (Figure **4-7**). 1 U/ml thrombin also significantly increased the phosphorylation ratio of occludin by 2.12 fold at time 30 minutes ($P<0.01$) and it then returned to 0.94 at time 120 minutes. This also paralleled the L_P response to thrombin (Figure **4-11**). Oscillatory shear stress of 10 ± 15 dyne/cm^2, which did not increase L_P (Figure **4-10**), showed a different time profile than the steady shear stress. The phosphorylation ratio significantly decreased to 0.74, 0.69, and 0.67 at times 15, 30, and 120 minutes, indicating different effects by steady and oscillatory shear stresses. In the L-NMMA and SNAP experiments (Figures **4-17** and **4-18**). 100 uM L-NMMA and 500 uM SNAP had no effect on L_p, whereas Western blotting of occludin after 3 hour exposure showed no change in the phosphorylation ratio in either experiment (Figure **4-20**). In all of these experiments, the phosphorylation ratio of occludin was highly correlated to the hydraulic conductivity, suggesting a role of phosphorylation of occludin in L_P regulation.

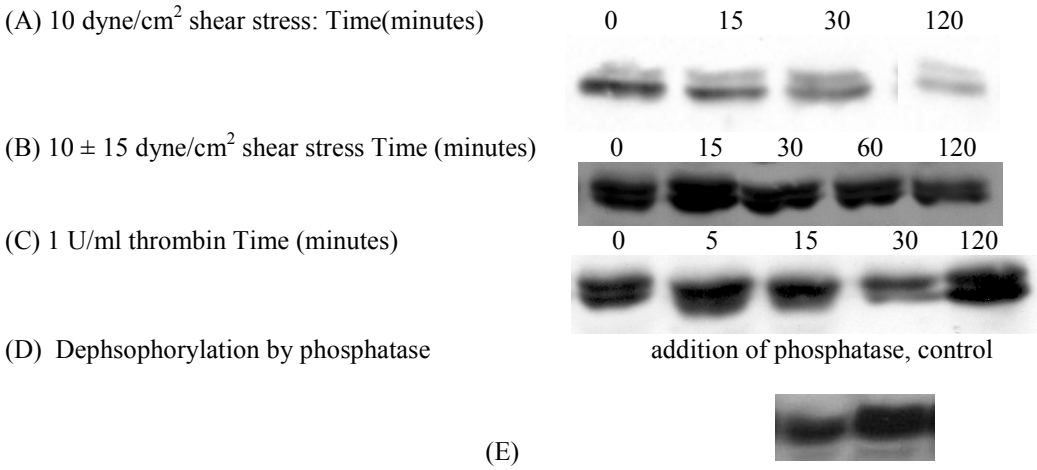

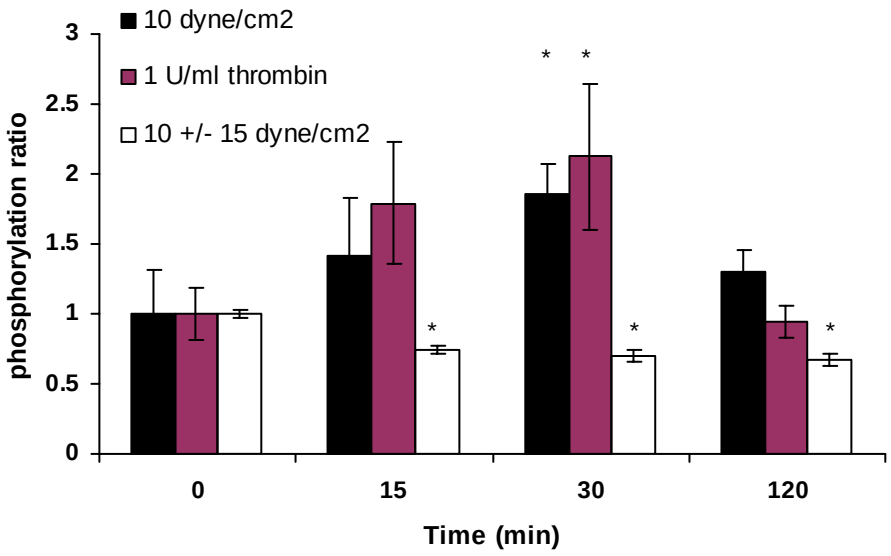

Figure **4-19**:Phosphorylation of occludin by 10 dyne/cm^2, 10 ± 15 dyne/cm^2, and 1 U/ml thrombin

N=3 for 10 dyne/cm^2, n=3 for 1 U/ml thrombin, and n=3 for 10 ± 15 dyne/cm^2
* denotes the significant difference with respect to values at time zero (*t-test*, P<0.05)

It should also be noted that the initial phosphorylation ratios differed in these experiments. At time 0, the phosphorylation ratio of occludin ranged from 0.35 to 1.16, reflecting the variation in cells. Therefore, all the phosphorylation ratios at other times were normalized to the phosphorylation ratio at time zero to eliminate the difference at the beginning of the experiments.

Figure **4-20**: L-NMMA and SNAP had no effect on HUVEC occludin phosphorylation

Western blotting of occludin at the end of L_P experiments. There was no change in occludin phosphorylation in both L-NMMA and SNAP experiments.(n=1)

However, shear stress did not change the total amount of occludin in the case of steady and oscillatory shear stresses (Figure **4-21**). There was no significant difference between later times and time zero. Application of 1 U/ml thrombin for 30 minutes significantly decreased the total amount of occludin while the phosphorylation ratio increased to 2.2, suggesting phosphorylation of occludin led to proteolysis of occludin. However, given only one data point, this is not conclusive.

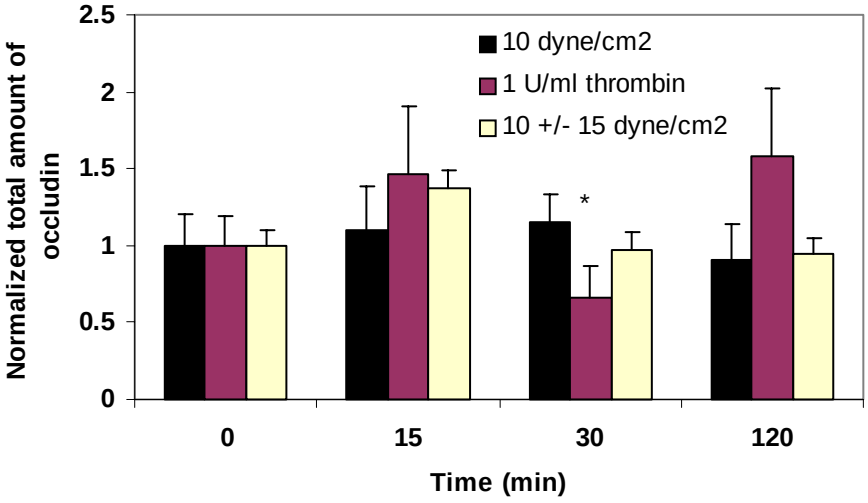

Figure **4-21**: Time profile of total amount of occludin by 10 dyne/cm^2, 10 ± 15 dyne/cm^2, and 1 U/ml thrombin.

N=3 for 10 dyne/cm^2, n=3 for 1 U/ml thrombin, and n=3 for 10 ± 15 dyne/cm^2
* denotes the significance with respect to time 0 (P=0.02)

Chapter 5

Discussion

5.1 In Vitro Study of Starling's Law

This study was the first to test the proposal of a modified Starling's law [11, 69]in an *in vitro* endothelial cell monolayer. We observed that the effective osmotic driving force under steady state conditions was substantially lower than predicted by Starling's law (Eq. **2.2**) using global concentrations, and that steady state reabsorption (negative flow) could not be observed even when the global osmotic gradient was substantially higher than the hydrostatic gradient. These observations are consistent with experiments in the microvessels of the frog mesentery [10, 16] and more general considerations of microvascular transport [70]. The results support the hypothesis that local concentrations, not global concentrations, determine the osmotic pressure differential[71].

To assess the steady state data, the model of Michel and Phillips[10] was used. The parameters L_P , P_d, and σ in Eqs. **2.4** and. **2.5** were assumed constant (independent of pressure and protein concentration) and were adjusted to minimize the square of the error between the predictions and the data. The resulting values of the parameters are: L_P =5.1 x 10^{-7} cm/sec/cmH_2O; P_d = 1.0 x 10^{-6} cm/s; σ = 0.71(dashed lines on Figure **4-2**). The L_P and P_d values are consistent with previous measurements of these parameters for BAEC monolayers *in vitro* [9, 57] and for porcine coronary arterioles *in vivo* [72]and the σ value is consistent with many *in vivo* measurements in capillaries[10, 72]. The

predicted Peclet numbers vary from 0.013 for the 5.5%-1% case at 5 cm H_2O up to 2.87 for 1%-1% case at 20 cm H_2O. The more sophisticated 3-dimensional model of Hu and Weinbaum[71], which focuses on the endothelial surface glycocalyx layer as the primary molecular sieve for plasma proteins, was not investigated.

We were unable to observe transient flow reversal when the luminal osmotic pressure was increased by adding a concentrated albumin solution to the luminal compartment. This would appear to be the result of slow equilibration of the osmotic solute with the endothelial layer due to transport limitations associated with the unstirred layer on the luminal surface of the endothelium.

In order to obtain a more rapid change in the overall Starling driving force, we equilibrated the system at 20 cm H_2O differential pressure with 5.5% BSA in the luminal compartment and then quickly dropped the pressure differential to 5 cm H_2O. We were able to observe a transient reversal which decayed rapidly during the first 30 seconds after the pressure change and was no longer observable after about 2 minutes (Figure **4-4**). A zero flow state then persisted for about 20 minutes before a positive steady state flow was finally established (Figure **4-3**). The dynamics of this reversal transient are similar to observations reported by Michel and Phillips [10]and Hu *et al*. [16]in frog mesenteric capillaries. They reported transient flow reversals during 5-20 second vessel occlusions and steady state positive flows after 2-5 minutes of occlusion. The time required to establish steady flow was somewhat longer in our *in vitro* experiments and may have been associated with the transport barrier provided by the supporting filter and the size of the abluminal chamber (20 cm^3).

A surprising finding of the present study was the asymmetry of the endothelial transport barrier *in vitro.* When hydrostatic pressure was used to reverse the direction of volumetric flux from the abluminal compartment to the luminal compartment, there was about a 100x increase in L_P (Table **4-1**). The *in vitro* endothelium, thus, has the characteristics of a check valve: high resistance to flow in one direction and low resistance in the opposite direction. Michel and Phillips [10] and Hu *et al.* [16] did not conduct experiments with the hydrostatic gradient reversed, but their transient osmotic reversal experiments suggested that the hydraulic conductivity was essentially the same in both flow directions, with no evidence of asymmetry. This difference in symmetry of the transport barrier is a distinct difference between the *in vitro* BAEC model and the frog mesenteric capillary model.

There was a previous report that albumin was transported in an asymmetric fashion across porcine pulmonary artery endothelium *in vitro* [73]. The transport of albumin from the abluminal to the luminal side was approximately ten-fold greater than transport from the luminal to the abluminal side. But Siflinger-Birnboim, *et al.* [74] were unable to confirm this finding in a similar system. Huxley and Curry reported asymmetry in barrier hydraulic conductivity with alterations in the albumin content of the luminal and abluminal sides of the blood vessel [75].

The elevated hydraulic conductivity that we observed for volume flux from the abluminal to the luminal compartment may have derived from the nature of the attachment of the endothelium to its basement matrix which must withstand fluid flow forces tending to cause separation when flow is the direction of reabsorption. When volume flux is in the normal filtration direction, fluid flow forces would tend to stabilize

this interface. It should also be noted that there was no "sealing effect" when the flow was in the direction of reabsorption either (Figure **4-5**). In fact, the hydraulic conductivity actually increased over time period of reverse flow. This further supports the notion that the change in direction of the pressure and flow forces is somehow responsible for the asymmetry of the transport barrier *in vitro*.

In spite of a significant difference in the symmetry of the endothelial transport barrier with respect to volume flux, the *in vitro* BAEC model and frog mesenteric capillaries display similar transport characteristics with respect to osmotic gradients. The fundamental observation in frog mesentery that an overall osmotic gradient favoring classical Starling reabsorption in fact produces steady state filtration is captured by the *in vitro* model. In addition, the dynamics of transient reabsorption are similar for both systems. The *in vitro* model, therefore, should continue to be useful for studies of the endothelial transport barrier when the hydrostatic pressure is highest on the luminal side of the barrier – the most common physiological situation.

5.2 Baseline HUVEC Transport Properties

In this study, we have utilized an established *in vitro* cell culture model to investigate hydraulic conductivity of cultured HUVEC monolayers and the mechanism mediating the effect of shear stress. The average L_P for HUVEC was about $3.2 \pm 0.58 \times 10^{-7}$ cm/sec/cmH_2O (n=16). In a separate study, Chang also reported a L_P of $3.55 \pm 0.39 \times 10^{-7}$ cm/sec/cmH_2O for HUVEC, which was close to the value we have measured. Luckett reported a L_P value of $2.9 \pm 0.86 \times 10^{-6}$ cm/sec/cm H_2O using cultured HUVEC monolayers on human amnion [76], which was an order of magnitude higher than observed here. The value measured in this study is the lowest value of HUVEC L_P reported, representing a tight monolayer, and close to the physiological values measured in many other *in vivo* studies.

In terms of the magnitude, HUVEC L_P showed no difference from BAEC L_P which ranged from 3.3×10^{-7} to 3.58×10^{-7} cm/sec/cmH_2O [9]. However, the appearance of some "giant cells" in HUVEC monolayers and their corresponding drifting baselines were the striking difference from BAEC monolayers and was the major technical difficulty encountered in this research. We believe that there was a correlation between the number of giant cells and the extent of the drifting baseline. As the passage number of cells became high, more and more giant cells appeared on cell monolayers and drifting of baseline became more severe. The source of "giant cells" might be related to damage to the cells during the process of primary culture and subsequent subcultures. Trypsin was the major problem, as evidenced by the following two facts: first, prolonged incubation with collagenase A or Blenzyme 2 containing trypsin or trypsin-like components resulted

in more giant cells; second, repeated treatment with trypsin led to an increased number of "giant cells" at high passages. We did not observe the appearance of "giant cells" in BAECs, indicating that HUVEC are more difficult to culture than other mammalian cells, and extra caution must be exercised. Trypsin was quickly removed by centrifuging for the subculture of HUVECs, while it was kept in the media during the subculture of BAECs.

5.3 Hydraulic Conductivity of HUVEC in Response to Shear Stress

To our knowledge, HUVEC hydraulic conductivity in response to shear stress was first reported in this study. Steady shear stress of 5, 10, or 20 dyne/cm^2 increased the baseline quickly followed by a return to control level (Figures **4-6** to Figure **4-8**). The duration of the transient state depended on the magnitude of the shear stress, but the peak elevation seemed to be independent of the magnitude of the shear stress.

The shear response displayed by HUVEC was very different from that of BAECs, which also showed a shear-induced hydraulic conductivity. In BAECs, Sill et al [8]reported that three hour exposure to steady shear stresses between 0.1 and 20.0 dyne/cm^2 revealed a threshold for shear-induced increase in L_P of 0.5 dyne/cm^2. At 20 dyne/cm^2, L_P initially decreased by 30 ± 13.4% ($P < 0.05$) and then increased to a level 3.76 ± 0.83-fold ($P < 0.05$) greater than control L_P at 3 h. However, the shear response of HUVEC showed a return to baseline within 2 hours after the onset of exposure to steady shear stress.

The effect of oscillatory shear stress was different from that of steady shear stress. Pure oscillatory shear stress of 0 ± 20 dyne/cm^2 exerted no effect on HUVEC Lp within 2

hours of application. Furthermore, the oscillatory components seemed to suppress the effect of steady shear stress. Superimposition of oscillatory shear stress of as little as 5 dyne/cm^2 to steady shear stress of 10 dyne/cm^2 was sufficient to suppress the transient increase induced by steady shear. Flow reversal was not necessary for oscillatory shear stress to take effect, whereas in BAEC only oscillatory shear stress with reversal was able to suppress the effect of steady shear stress. Oscillatory shear stress with no reversal, 10 ± 10 dyne/cm^2, increased BAEC L_P by 3 fold within 90 minutes [18], whereas same oscillatory shear stress induced no effect on HUVEC L_P (Figure **4-10**). The different effects of steady and oscillatory shear stresses on HUVEC L_P imply that there might be separate receptors and signal transduction pathways for steady and oscillatory shear stresses.

5.4 Mechanism of Hydraulic Conductivity Regulation

5.4.1 Calcium pathway is involved in HUVEC hydraulic conductivity regulation, but shear response seems to be calcium-independent

Intracellular calcium seems to regulate the hydraulic conductivity of HUVEC. There are two lines of evidence supporting this idea. First, the addition of BAPTA-AM, abolishing intracellular calcium, reduced monolayer L_P values significantly (Figure **4-14**). Second, pre-incubation with BAPTA-AM inhibited the rise of L_P induced by thrombin (Figure **4-12**). The delayed response of L_P induced by BAPTA-AM confirmed the requirement of Ca^{2+} signaling in the mechanism of thrombin-induced increase in endothelial permeability [49]. The eventual increase of the baseline after 30 minutes of treatment with thrombin in the presence of BATPA-AM might be the result of consumption of all of the BAPTA-AM by thrombin-induced calcium. However, the failure of BAPTA-AM to block the shear response in HUVEC (Figure **4-13**) indicated that shear affects Lp through a calcium-independent pathway.

Intracellular calcium also affects BAEC L_P. Addition of Ca^{2+} ionophore, A 23187, caused a significant increase in BAEC Lp. Further, chelation of extracellular Ca^{2+} with EGTA attenuated the shear-L_P response, providing some support for the importance of Ca^{2+} in mediating the shear-induced increase in BAEC L_P. However, the intracellular chelator, EGTA-AM had no significant effect in attenuating the shear response,

suggesting that intracellular calcium is not important in the shear response in BAEC either [58].

There are other processes besides the calcium dependent mechanism that might regulate cell permeability in response to shear stress. Several other studies have reported calcium-independent pathways for increased permeability. In the case of HUVEC albumin permeability response to bradykinin (BK), intracellular calcium concentration and F-actin were not changed. Ehringer et al hypothesized that BK may increase HUVEC permeability by producing matrix metalloproteinase-2 [77]. He *et al.* found cGMP modulated basal and activated microvessel permeability independent of Ca^{2+}. [78] Finally, suppression of NO formation using NOS inhibitor, L-NMMA or L-NAME, increased hydraulic conductivity without any change in Ca^{2+} [58, 79], and an increase in oxidative stress appeared to be a mechanism for increased hydraulic conductivity. Ayajiki [80]reported in native endothelial cells (rabbit iliac artery), that shear stress induced nitric oxide production through intracellular pH and tyrosine phosphorylation but not calcium pathway.

In this study, we did not chelate the extracellular calcium. It is well-known that adhesion of endothelial cells to the matrix needs the presence of calcium. The depletion of extracellular calcium leads to cell detachment from the matrix, thereby significantly increasing the hydraulic conductivity of cell monolayer to a non-physiological value.

5.4.2 Hydraulic conductivity is independent of NO pathway

Shear stress increased cumulative NO (precisely nitrite) concentrations (Figure **4-15**). Regarding NO production in BAEC and HUVEC, some differenced are noted here, especially for the oscillatory shear. Oscillatory shear (10 ± 15 dyne/cm^2) dramatically increased NO concentration by 14 fold after three hours exposure in BEAC [18], but in HUVEC 10 ± 15 dyne/cm2 elicited NO concentration up to 4 fold only, not significantly different from the effect of 10 and 20 dyne/cm^2 steady shear stress. These results are consistent with Ziegler's observation, where he noticed that unidirectional (not steady) shear stress increases eNOS mRNA expression in both BAEC and Eahy926 (a hybridoma cell line obtained by fusing HUVEC and human carcinoma cell line A549), while oscillatory shear stress (-3 3) slightly upreguated eNOS mRNA in BAEC whereas it downregulated eNOS mRNA in Eahy926 [81].

However, the hydraulic conductivity of HUVEC did not increase in response to elevated NO production. Addition of SNAP to HUVEC did not have any effect on HUVEC L_P (Figure **4-16**), and neither did blocking NO production with L-NMMA (Figure **4-17**). Apparently the proteins regulating transport pathway are not controlled by the NO signal transduction pathway. In BAEC, shear-induced hydraulic conductivity was dependent on NO, as evidenced by the following two facts: first SNAP increased endothelial L_P by 2.23 ± 0.14-fold (100 micromol/L) and 4.8 ± 0.66-fold (500 micromol/L) at the end of 3 hours. In addition, BAEC exposed to NOS inhibitors, N^G-monomethyl-L-arginine and N^G-nitro-L-arginine methyl ester, exhibited significant attenuation of shear-induced increase in L_P in a dose-dependent manner [58]. Although

HUVEC produce NO in response to shear stress, a mechanism downstream of No that would alter junction proteins and in turn L_P, appears to be missing in HUVEC.

5.5 Ocludin Phosphorylation and Regulation of Cell Permeability

Occludin is possibly involved in the regulation mechanism of the tight junction at two distinct levels: the transcriptional level (mRNA and protein expression) and the posttranslational level (phosphorylation). It has been reported that occludin has different phosphorylated states from non-phosphorylated to diphosphorylated [82]. In this study, two phosphorylation states were observed, namely, dephosphorylated and phosphorylated states with molecular weights at 59 and 61 kDa, respectively (Figure **4-19**).

Conklin [83]reported the effect of shear stress on occludin in the excised porcine carotid artery. Lower shear stress (1.5 dyne/cm^2) compared to physiological shear stress (15 dyne/cm^2), decreased occludin mRNA and protein expression, causing increased permeability. In other words, high shear stress increased occludin expression and lowered permeability. However, they did not investigate the phosphorylation of the occludin. In BEAC, DeMaio [59] showed an opposite effect of shear stress on occludin expression in BAEC, where total content of occludin decreased as shear stress increased. In HUVEC in the present study, the total amount of occludin remained unchanged, while HUVEC Lp increased transiently.

HUVEC L_P reached a peak value 5 minutes after the addition of thrombin at 1 U/ml (fig). This time pattern was very similar to F-actin formation reported in HUVEC[84]. 0.3 U/ml thrombin induced a rapid (within 5 minutes) increase (1.7 fold) in

the number of microfilaments in HUVECs and persisted for at least 30 minutes. The thrombin-induced increase in actin fiber is reversible. HUVECs treated for 5 minutes with thrombin, followed by normal buffer, showed a normal actin pattern 20 to 30 minutes after removal of thrombin. A new finding in this study is that thrombin also increased occludin phosphorylation. Therefore, the increase of permeability after the treatment with thrombin was at least partially due to the alteration of the tight junction. However, we are still unable to determine the relative importance of the cytoskeleton and tight junctions in regulating the permeability.

Occludin phosphorylation seems to lead to proteolysis of occludin, thus resulting in disintegration of tight junction and increase of permeability. DeMaio [59] reported that 10 and 20 dyne/cm^2 shear stress increased phosphorylation states and decreased total content of occludin, which was consistent with this hypothesis. Wachtel [68]reported that inhibition of phosphatase led to elevation of permeability also confirmed this hypothesis. In this study, the maximum increase in the phosphorylation of occludin by 1 U/ml thrombin after 30 minutes occurred simultaneously with a significant reduction of total content of occludin, providing another evidence.

Occludin phosphorylation is highly correlated with the hydraulic conductivity, as shown by following lines of evidence. First, steady shear stress (10 dyne/cm^2) elevated occludin phosphorylation during the first 30 minutes and the phosphorylation state returned to normal after that, which is coincident with the hydraulic conductivity profile in response to shear stress (compare Figures **4-7** and **4-19E**). Second, oscillatory shear stress (10 ± 15 dyne/cm^2) decreased occludin phosphorylation, resulting in no change on hydraulic conductivity (compare Figures **4-10** and **4-19E**). Third 1 U/ml thrombin

increased occludin phosphorylation transiently, which was corresponding to its hydraulic conductivity responses (compare Figures **4-11** and **4-19E**). Last, L-NMMA and SNAP had no effect on occludin phosphorylation, and hence no effect on L_P (compare Figures **4-16**, **4-17**, and **4-20**).

A close exam of two time profiles of occludin phosphorylation and L_P response to steady shear stress and thrombin shows that there is a time dalay in occludin phosphorylation with respect to L_P response, indicating that occludin may not be the only regulator for the hydraulic conductivity and that other proteins may also play a role.

Although two cell types (HUVECs and BAECs) have different L_P responses to shear stress and signal transduction pathways, a common feature is the phosphorylation of occludin, namely, the phosphorylation of occludin induces an increase in hydraulic conductivity. Steady shear stress irreversibly increases the occludin phosphorylation in BAECs, corresponding to a sustained elevation in L_P, whereas it only transiently increases the occludin phosphorylation in HUVECs, corresponding to a transient increase in L_P, suggesting that occludin phosphorylation may be a common feature controlling the permeability response to shear stress in other vessels in the cardiovascular system.

Table **5-1** shows a summary comparison of shear stress effects on HUVEC L_P and BAEC L_P and their underlying mechanism.

Table **5-1**: **Comparison of HUVEC and BAEC transport properties and their underlying mechanisms**

	HUVEC	BAEC
Transport properties		
Steady shear stress 20, 10, 5 dyne/cm^2	Transiently increased L_P and then return to control	Sustained increase in L_P
Oscillatory shear stress		
Non-reversing 10 ± 5, 10 ± 10 dyne/cm^2	Suppressed effect of steady shear stress on L_P	Did not suppress
Reversing 10 ± 15 dyne/cm^2	Same as non-reversing	Suppressed the effect of steady shear stress
Signal transduction pathway		
Intracellular calcium	Seemed to be involved in the regulation of hydraulic conductivity, however, chelating of intracellular calcium showed no effect on shear response of HUVEC or BAEC, indicating that the shear response was independent of intracellular calcium	
NO pathway		
NO concentration	Increased by shear in HUVEC and BAEC	
SNAP (500 uM)	No effect on L_P	Increase L_P
L-NMMA (100 uM)	No effect on L_P	Decrease L_P
Occludin phosphorylation		
Total content of occludin	No change by shear	Decreased by shear
Phosphorylation states	Increased transiently by shear and then return to control	Increased by shear

Chapter 6

Future work

In this study, we have established that shear stress affected L_P through an NO independent or calcium independent pathway, indicating that other signal transduction pathways are responsible for this process. Other signal transduction pathways such as cAMP, cGMP, and their cross-talks will be investigated in the future study.

In this study, we also established that occludin is one of the big players in the regulation of L_P in HUVECs and BAECs. Although we have linked occludin phosphorylation to the increase of hydraulic conductivity, it is still unclear what signaling pathway mediates the phosphorylation of occludin in HUVECs, especially what protein kinases phosphorylate occludin and which amino acid of occludin is phosphorylated. It has been observed that application of protein tyrosine phosphatase inhibitor, phenylarsine oxide (PAO) and pervanadate, resulted in proteolysis of the occludin, leading to the formation a cleavage product of 50 kDa and elevated permeability for FITC-dextran. However, the role of tyrosine phosphorylation in the control of proteolysis was still inconclusive, since probing immunoprecipiated occludin from HUVECs for phosphotyrosince revealed no signal under PAO treatment [68]. The search of protein kinases for occludin phosphorylation should continue in the future study.

Adherens junctions may also contribute to the permeability. Shear stress caused a transient reorganization of adherens junction proteins -- catenins, VE-cadherins and plakoglobins. Furthermore, disruption of the adherens junction protein cadherins leads to

the opening of tight junctions. Western blotting of protein levels indicated that 15-50 dyne/cm^2 shear stress led to a decrease in α-catenin and VE-cadherin after 8.5 hour exposure to flow, followed by an increase back to pre-shear value [27, 28]. The combined study of tight junctions and adherens junctions may eventually unveil the mechanism of permeability regulation in ECs.

A fundamental question remains unanswered here, namely, what is the mechanosensor for the shear stress. The preliminary study in our lab has suggested that the glycocalyx layer covering endothelial cells may act as a mechanosensor relaying the signal from shear stress. The incubation with heparinase (10 U/ml) to partially remove the glycocalyx resulted in an increase in L_P (data not shown), providing some evidence supporting the role of glycocalyx in EC hydraulic conductivity. However, more research should be conducted to pursue this end.

Finally, we limited our study on L_P, which only represents the transport of water and small molecules through paracellular pathway. In order to understand the transport of large molecules such as albumin and LDLs, their permeability (*Pe*) should be measured simultaneously with L_P to investigate the contributions of the paracellular pathway and the transcellular pathway (through vesicle transport). A new system measuring L_P and Pe simultaneously has been developed in our lab, and will prove to be useful in the future research.

Reference

1. Lever, M.J., J.M. Tarbell, and C.G. Caro, *The effect of luminal flow in rabbit carotid artery on transmural fluid transport.* Exp Physiol, 1992. 77(4): p. 553-63.
2. Yuan, Y., et al., *Flow modulates coronary venular permeability by a nitric oxide-related mechanism.* Am J Physiol, 1992. 263(2 Pt 2): p. H641-6.
3. Shibata, M. and A. Kamiya, *Blood flow dependence of local capillary permeability of Cr-EDTA in the rabbit skeletal muscle.* Jpn J Physiol, 1992. 42(4): p. 631-9.
4. Friedman, M.H., et al., *Shear-dependent thickening of the human arterial intima.* Atherosclerosis, 1986. 60(2): p. 161-71.
5. Ku, D.N., et al., *Pulsatile flow and atherosclerosis in the human carotid bifurcation. Positive correlation between plaque location and low oscillating shear stress.* Arteriosclerosis, 1985. 5(3): p. 293-302.
6. Nerem, R.M. and M. Levesque, *Fluid mechanics in atherosclerosis*, in *Handbook of bioengineering*, R. Skalak and S. Chien, Editors, McGraw-Hill Book company.
7. Williams, D.A., *Network assessment of capillary hydraulic conductivity after abrupt changes in fluid shear stress.* Microvasc Res, 1999. 57(2): p. 107-17.
8. Sill, H.W., et al., *Shear stress increases hydraulic conductivity of cultured endothelial monolayers.* Am J Physiol, 1995. 268(2 Pt 2): p. H535-43.
9. Chang, Y.S., et al., *Effect of vascular endothelial growth factor on cultured endothelial cell monolayer transport properties.* Microvasc Res, 2000. 59(2): p. 265-77.

10. Michel, C.C. and M.E. Phillips, *Steady-state fluid filtration at different capillary pressures in perfused frog mesenteric capillaries.* J Physiol, 1987. 388: p. 421-35.

11. Weinbaum, S., *1997 Whitaker Distinguished Lecture: Models to solve mysteries in biomechanics at the cellular level; a new view of fiber matrix layers.* Ann Biomed Eng, 1998. 26(4): p. 627-43.

12. Starling, E.H., *On the adsorption of luids from connective tissue spaces.* J. Physiology, 1896. 19: p. 312-326.

13. Berne, R. and M. Levey, *Physiology*. 1998, St. Louis: Mosby, Inc.

14. Intaglietta, M. and B. Zweifach, *Microcirculatory basis of fluid exchange*, in *Advances in Biological and Medical Physics*, J. Lawrence and G. JW, Editors. 1974, Academic Press.

15. Patlak, C.S., D.A. Goldstein, and J.F. Hoffman, *The flow of solute and solvent across a two-membrane system.* J Theor Biol, 1963. 5(3): p. 426-42.

16. Hu, X., et al., *Starling forces that oppose filtration after tissue oncotic pressure is increased,* Am J Physiol Heart Circ Physiol, 2000. 279(4): p. H1724-36.

17. Tarbell, J.M., L. Demaio, and M.M. Zaw, *Effect of pressure on hydraulic conductivity of endothelial monolayers: role of endothelial cleft shear stress.* J Appl Physiol, 1999. 87(1): p. 261-8.

18. Hillsley, M.V. and J.M. Tarbell, *Oscillatory shear alters endothelial hydraulic conductivity and nitric oxide levels.* Biochem Biophys Res Commun, 2002. 293(5): p. 1466-71.

19. Tarbell, J.M., *Mass Transport in Arteries and the Localization of Atherosclerosis.* Annu Rev Biomed Eng, 2003. 19: p. 19.

20. Alberts, B., et al., *Molecular biology of cells*. 3rd ed. 1996, New York & London: Garland Publishing, Inc.

21. Garcia, J.G., H.W. Davis, and C.E. Patterson, *Regulation of endothelial cell gap formation and barrier dysfunction: role of myosin light chain phosphorylation.* J Cell Physiol, 1995. 163(3): p. 510-22.

22. Wysolmerski, R.B. and D. Lagunoff, *Regulation of permeabilized endothelial cell retraction by myosin phosphorylation.* Am J Physiol, 1991. 261(1 Pt 1): p. C32-40.

23. Levesque, M.J. and R.M. Nerem, *The elongation and orientation of cultured endothelial cells in response to shear stress.* J Biomech Eng, 1985. 107(4): p. 341-7.

24. Phillips, P.G., et al., *Phallacidin prevents thrombin-induced increases in endothelial permeability to albumin.* Am J Physiol, 1989. 257(3 Pt 1): p. C562-7.

25. Lum, H. and A.B. Malik, *Regulation of vascular endothelial barrier function.* Am J Physiol, 1994. 267(3 Pt 1): p. L223-41.

26. Dejana, E., M. Corada, and M.G. Lampugnani, *Endothelial cell-to-cell junctions.* Faseb J, 1995. 9(10): p. 910-8.

27. Noria, S., et al., *Transient and steady-state effects of shear stress on endothelial cell adherens junctions.* Circ Res, 1999. 85(6): p. 504-14.

28. Seebach, J., et al., *Endothelial barrier function under laminar fluid shear stress.* Lab Invest, 2000. 80(12): p. 1819-31.

29. Furuse, M., et al., *Occludin: a novel integral membrane protein localizing at tight junctions.* J Cell Biol, 1993. 123(6 Pt 2): p. 1777-88.

30. Stevenson, B.R., et al., *Identification of ZO-1: a high molecular weight polypeptide associated with the tight junction (zonula occludens) in a variety of epithelia.* J Cell Biol, 1986. 103(3): p. 755-66.

31. Gumbiner, B., T. Lowenkopf, and D. Apatira, *Identification of a 160-kDa polypeptide that binds to the tight junction protein ZO-1.* Proc Natl Acad Sci U S A, 1991. 88(8): p. 3460-4.

32. Citi, S., et al., *Cingulin, a new peripheral component of tight junctions.* Nature, 1988. 333(6170): p. 272-6.

33. Zhong, Y., et al., *Monoclonal antibody 7H6 reacts with a novel tight junction-associated protein distinct from ZO-1, cingulin and ZO-2.* J Cell Biol, 1993. 120(2): p. 477-83.

34. Keon, B.H., et al., *Symplekin, a novel type of tight junction plaque protein.* J Cell Biol, 1996. 134(4): p. 1003-18.

35. Hirase, T., et al., *Occludin as a possible determinant of tight junction permeability in endothelial cells.* J Cell Sci, 1997. 110(Pt 14): p. 1603-13.

36. Tio, S., M. Deenen, and E. Marani, *Astrocyte-mediated induction of alkaline phosphatase activity in human umbilical cord vein endothelium: an in vitro model.* Eur J Morphol, 1990. 28(2-4): p. 289-300.

37. Stevenson, B.R. and D.A. Begg, *Concentration-dependent effects of cytochalasin D on tight junctions and actin filaments in MDCK epithelial cells.* J Cell Sci, 1994. 107(Pt 3): p. 367-75.

38. Hsieh, H.J., N.Q. Li, and J.A. Frangos, *Shear-induced platelet-derived growth factor gene expression in human endothelial cells is mediated by protein kinase C.* J Cell Physiol, 1992. 150(3): p. 552-8.

39. Olesen, S.P., D.E. Clapham, and P.F. Davies, *Haemodynamic shear stress activates a K+ current in vascular endothelial cells.* Nature, 1988. 331(6152): p. 168-70.

40. Hsieh, H.J., N.Q. Li, and J.A. Frangos, *Pulsatile and steady flow induces c-fos expression in human endothelial cells.* J Cell Physiol, 1993. 154(1): p. 143-51.

41. Harrison, V.J., et al., *Endothelin-1 and endothelin-converting enzyme-1 gene regulation by shear stress and flow-induced pressure.* J Cardiovasc Pharmacol, 1998. 31(Suppl 1): p. S38-41.

42. Kuchan, M.J. and J.A. Frangos, *Shear stress regulates endothelin-1 release via protein kinase C and cGMP in cultured endothelial cells.* Am J Physiol, 1993. 264(1 Pt 2): p. H150-6.

43. Helmke, B.P. and P.F. Davies, *The cytoskeleton under external fluid mechanical forces: hemodynamic forces acting on the endothelium.* Ann Biomed Eng, 2002. 30(3): p. 284-96.

44. Busse, R. and A. Mulsch, *Calcium-dependent nitric oxide synthesis in endothelial cytosol is mediated by calmodulin.* FEBS Lett, 1990. 265(1-2): p. 133-6.

45. Xiao, Z., et al., *Shear stress induction of the endothelial nitric oxide synthase gene is calcium-dependent but not calcium-activated.* J Cell Physiol, 1997. 171(2): p. 205-11.

46. Sigurdson, W.J., F. Sachs, and S.L. Diamond, *Mechanical perturbation of cultured human endothelial cells causes rapid increases of intracellular calcium.* Am J Physiol, 1993. 264(6 Pt 2): p. H1745-52.

47. Brakemeier, S., et al., *Up-regulation of endothelial stretch-activated cation channels by fluid shear stress.* Cardiovasc Res, 2002. 53(1): p. 209-18.

48. Bogatcheva, N.V., J.G. Garcia, and A.D. Verin, *Molecular mechanisms of thrombin-induced endothelial cell permeability.* Biochemistry (Mosc), 2002. 67(1): p. 75-84.

49. Sandoval, R., et al., *Requirement for Ca2+ signaling in the mechanism of thrombin-induced increase in endothelial permeability.* Am J Physiol Lung Cell Mol Physiol, 2001. 280(2): p. L239-47.

50. Kuchan, M.J. and J.A. Frangos, *Role of calcium and calmodulin in flow-induced nitric oxide production in endothelial cells.* Am J Physiol, 1994. 266(3 Pt 1): p. C628-36.

51. Nishida, K., et al., *Molecular cloning and characterization of the constitutive bovine aortic endothelial cell nitric oxide synthase.* J Clin Invest, 1992. 90(5): p. 2092-6.

52. Meyer, D.J., Jr. and V.H. Huxley, *Differential sensitivity of exchange vessel hydraulic conductivity to atrial natriuretic peptide.* Am J Physiol, 1990. 258(2 Pt 2): p. H521-8.

53. Rumbaut, R.E., M.K. McKay, and V.H. Huxley, *Capillary hydraulic conductivity is decreased by nitric oxide synthase inhibition.* Am J Physiol, 1995. 268(5 Pt 2): p. H1856-61.

54. Kubes, P. and D.N. Granger, *Nitric oxide modulates microvascular permeability.* Am J Physiol, 1992. 262(2 Pt 2): p. H611-5.

55. Kurose, I., et al., *Inhibition of nitric oxide production. Mechanisms of vascular albumin leakage.* Circ Res, 1993. 73(1): p. 164-71.

56. Jo, H., et al., *Endothelial albumin permeability is shear dependent, time dependent, and reversible.* Am J Physiol, 1991. 260(6 Pt 2): p. H1992-6.

57. Dull, R.O., et al., *The effect of varying albumin concentration and hydrostatic pressure on hydraulic conductivity and albumin permeability of cultured endothelial monolayers.* Microvasc Res, 1991. 41(3): p. 390-407.

58. Chang, Y.S., et al., *Shear-induced increase in hydraulic conductivity in endothelial cells is mediated by a nitric oxide-dependent mechanism.* Arterioscler Thromb Vasc Biol, 2000. 20(1): p. 35-42.

59. DeMaio, L., et al., *Shear stress regulates occludin content and phosphorylation.* Am J Physiol Heart Circ Physiol, 2001. 281(1): p. H105-13.

60. Sill, H.W., et al., *Albumin permeability and electrical conductivity as means of assessing endothelial cell monolayer integrity.* Journal of Tissue Culture Methods, 1992. 14: p. 253-258.

61. Jaffe, E.A., et al., *Culture of human endothelial cells derived from umbilical veins: identification by morphologic and immunologic criteria.* J. Clin. Invest., 1973. 52: p. 2745-2756.

62. Nims, R.W., *Methods in Enzymology*. Vol. 268. 1996. 93.

63. Misko, T.P., et al., *A fluorometric assay for the measurement of nitrite in biological samples.* Anal Biochem, 1993. 214(1): p. 11-6.

64. Lowry, O.H., et al., *Protein measurement with the Folin Phenol Reagent.* J. Biol. Chem., 1951. 193: p. 265-275.

65. Laemmli, U., *Cleavage of structural proteins during the assembly of the head of bateriophage T4.* Nature, 1970. 227: p. 680-685.

66. Tarbell, J.M., M.J. Lever, and C.G. Caro, *The effect of varying albumin concentration of the hydraulic conductivity of the rabbit common carotid artery.* Microvasc Res, 1988. 35(2): p. 204-20.

67. Kuchan, M.J., H. Jo, and J.A. Frangos, *Role of G proteins in shear stress-mediated nitric oxide production by endothelial cells.* Am J Physiol, 1994. 267(3 Pt 1): p. C753-8.

68. Wachtel, M., et al., *Occludin proteolysis and increased permeability in endothelial cells through tyrosine phosphatase inhibition.* J Cell Sci, 1999. 112(Pt 23): p. 4347-56.

69. Michel, C.C., *Starling: the formulation of his hypothesis of microvascular fluid exchange and its significance after 100 years.* Exp Physiol, 1997. 82(1): p. 1-30.

70. Levick, J.R., *Capillary filtration-absorption balance reconsidered in light of dynamic extravascular factors.* Exp Physiol, 1991. 76(6): p. 825-57.

71. Hu, X. and S. Weinbaum, *A new view of Starling's hypothesis at the microstructural level.* Microvasc Res, 1999. 58(3): p. 281-304.

72. Huxley, V.H. and D.A. Williams, *Basal and adenosine-mediated protein flux from isolated coronary arterioles.* Am J Physiol, 1996. 271(3 Pt 2): p. H1099-108.

73. Shasby, D.M. and M.W. Peterson, *Effects of albumin concentration on endothelial albumin transport in vitro.* Am J Physiol, 1987. 253(3 Pt 2): p. H654-61.

74. Siflinger-Birnboim, A., et al., *Involvement of Ca2+ in the H2O2-induced increase in endothelial permeability.* Am J Physiol, 1996. 270(6 Pt 1): p. L973-8.

75. Huxley, V.H. and F.E. Curry, *Effect of superfusate albumin on single capillary hydraulic conductivity.* Am J Physiol, 1987. 252(2 Pt 2): p. H395-401.

76. Luckett, P.M., et al., *Hydraulic conductivity of endothelial cell monolayers cultured on human amnion.* Am J Physiol, 1989. 256(6 Pt 2): p. H1675-83.

77. Ehringer, W.D., et al., *Bradykinin and alpha-thrombin increase human umbilical vein endothelial macromolecular permeability by different mechanisms.* Inflammation, 2000. 24(2): p. 175-93.

78. He, P., M. Zeng, and F.E. Curry, *cGMP modulates basal and activated microvessel permeability independently of [Ca2+]i.* Am J Physiol, 1998. 274(6 Pt 2): p. H1865-74.

79. He, P., M. Zeng, and F.E. Curry, *Effect of nitric oxide synthase inhibitors on basal microvessel permeability and endothelial cell [Ca2+]i.* Am J Physiol, 1997. 273(2 Pt 2): p. H747-55.

80. Ayajiki, K., et al., *Intracellular pH and tyrosine phosphorylation but not calcium determine shear stress-induced nitric oxide production in native endothelial cells.* Circ Res, 1996. 78(5): p. 750-8.

81. Ziegler, T., et al., *Nitric oxide synthase expression in endothelial cells exposed to mechanical forces.* Hypertension, 1998. 32(2): p. 351-5.

82. Sakakibara, A., et al., *Possible involvement of phosphorylation of occludin in tight junction formation.* J Cell Biol, 1997. 137(6): p. 1393-401.

83. Conklin, B.S., et al., *Shear stress regulates occludin and VEGF expression in porcine arterial endothelial cells.* J Surg Res, 2002. 102(1): p. 13-21.

84. Thurston, G. and D. Turner, *Thrombin-induced increase of F-actin in human umbilical vein endothelial cells.* Microvasc Res, 1994. 47(1): p. 1-20.

85. Davies, P.F., T. Mundel, and K.A. Barbee, *A mechanism for heterogeneous endothelial responses to flow in vivo and in vitro.* J Biomech, 1995. **28**(12): p. 1553-60.

Appendix A

Primary Culture of Human Umbilical Vein Endothelial Cells

Media Preparation

Buffers and Media
HBSS solution
EGM
Collagenase solution
50 ml DPBSS
1%(v/v) 200 mM $CaCl_2$ =0.5 ml
collagenase powder final conc. 0.02% (w/v) =10 mg
stir for 30 min at room temperature, centrifuge at 2000g, and filter the supernant through 0.45 um filter.

Procedure :

All procedures are to be carried out in the laminar flow hood!!! Use good aseptic technique. All waste, except viable cord tissue, is to be placed in a biohazard bag.

Cord preparation

1. Place all items in hood, all items should be sprayed generously with 70% ethanol prior to placing in the laminar flow hood.
2. Remove the cords from bags, Sort the collected cord (about 10-25 cm long)
   Keep only white/slightly yellow, non-clotted, long cords. Red tinge to tissue, dark coloration is bad. Swelling/pocket of swelling (potential amniotic fluid) is bad
3. Clean cords with Kimwipes, lay out good cords on the absorbing tissue in the hood, non-sterile gloves could be used during this step.
4. Open a sterile glove package in the hood and lay flat on the absorbing tissue, put the sterile gloves on and transfer the cords onto the paper wrapping that the gloves came in.
5. Trim the cords for catheterization
   Cut 1/4-1/2" inch or as much of the cord as necessary to avoid clots/bad tissue, try to avoid stretched or "floppy" cords
6. Catherterization- Be sure you insert into the vein (make a clean transverse cut across one end of the cord to expose the two umbilical arteries and umbilical vein, the latter can be identified by its thinner wall and larger stretchable lumen)

- Push down onto work surface, hold with fingers, and slowly insert catheter into vein, up to smooth neck of catheter.
- Get cable ties, attach at smooth spot, push to collar
- Complete tightening tie with tensioning device, fit each catheter with a one-way stopcock

Blood removal & collagenase incubation

7. Pour 600 ml of pre-heated HBSS into 1 L beaker, Fill 60cc syringe with HBSS, attach to catheter and open stopcock.
8. Insert end of cord into the neck of 1 L bottle, and begin carefully injecting HBSS into cord until you see HBSS and blood to run into bottle
9. Run cord until no blood is seen, only HBSS. (about 50 ml HBSS for each cord)
10. Inject pre-warmed, pre-diluted collagenase into the cord and perfuse the cord until last trace of the red-colored HBSS has come out, clamp the end of the cord with a hemostat and continue filling the cords with collagenase solution until slight distension, close the stopcock. Let it sit for 45 min.

Cell collection

11. Put on a new sterile glove, attach 60cc HBSS syringe to catheter, and begin to gently agitate the cord to release the cells, agitate cord by gently rolling the cord on the work surface and also by manually palpitating the cord with your finger.
12. Insert the end of the cord in the neck of the bottle, open the stopcock and begin squeezing the collagenase out of the cord.
13. Open the stopcock and begin injecting HBSS into cord. Rinse cord several times with warm HBSS and discard cord when through.(about 50 ml)

Cell isolation

14. Pipette the eluted fluid into the appropriate # of 50 ml conicals, Be careful to avoid clots when pipetting
15. Spin the cells down in the centrifuge for 10 min at 1000 rpm (set to "1"), (650g)

Seeding slides

16. Pull off the supernatant from 50 ml conicals, being careful not to disturb the pellet at the bottom of tube.
17. Add enough pre-warmed EGM 10 ml to the conicals to seed, transfer the cell-suspension to a T25 flask and incubate overnight.
18. Rinse the flask with DPBSS or HBSS to remove non-adherent blood cell and add fresh EGM, the resulting plating density is 1.5-3.5* 10-4 cells/cm (confluence is normally reached after 2-3 days)----the next day, remove the medium from the T25, rinse the cells with pre-warmed serum free medium to remove any residual red cells and add 4 ml fresh culture medium.
19. Every second day, feed the cells by removing and discard half of the medium in the flask and replaced it with fresh serum-containing culture medium, the cells should

reach confluence in 7 days or less and be ready for use, or they can be subcultured to obtain a large number of cells.

Disposal of human umbilical cords

After harvesting cells, the used umbilical cords are put in a sealed biohazard bag and stored in a -20^{o}C freezer. The staff from University Office of Environmental Health and Safety picks them up and cords are finally incinerated. The liquid waste is treated with bleach for 30 minutes before disposal. All the other waste is collected in a special container labeled with " Human tissue only" and autoclaved at 120 ^{o}C before discarding.

Note: serum contains a trypsin inhibitor, so in some case, we must use serum free medium.

Reference:

David M.L. Morgan, Isolation and culture of human umbilical vein endothelial cells, in *Human cell culture protocols* (Gareth E. Jones, eds). Humana Press, Totowa, NJ, 101-110, 1996.

Appendix B

Purity of HUVECs Using Flow Cytometry

PENN STATE FLOW CYTOMETRY

COULTER(R) EPICS(R) Acquisition Flow Cytometry Report

19Jul00 16:07:26
LDL
G0092043
ps A2 1X

OP ID: SORDILLO

196 seconds, 10919 events

Ini[illegible]ytosett. from prot. LDL

Stop Count: 10000 events, histogram 2

1:

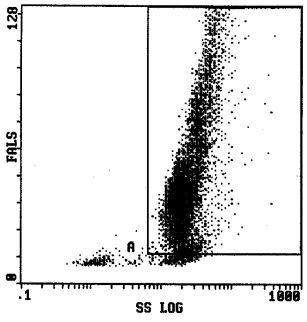

2: A

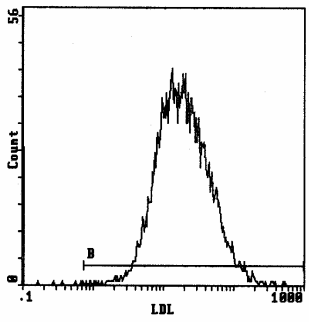

3:

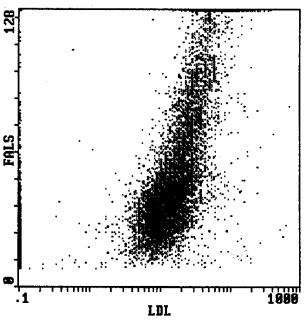

Stats: Not Normalized, Listgating: Disabled

Hist	Region ID	%	Count	Mn X	Mn Y	PkPosX	PkPosY	PkCnt	FPCVX	FPCVY
1	A A	91.6	10000	29.7	57.9	71.5	127.0	73	61.75	56.30

Hist	Region ID	%	Count	Mn X	Md X	PkPosX	PkCnt	HPCV	Min	Max
2	B B	93.8	9385	19.8	19.0	21.2	55	10.50	0.754	1024

XL Z18142 (3.0/1.23)

Page 1

VITA
Zhengyu Pang

EDUCATION

The Pennsylvania State University, University Park, PA 16803
Ph.D in Chemical Engineering, 2003

East China University of Science and Technology, Shanghai, China
M.S. in Biochemical Engineering, 1996

Nanjing University of Chemical Technology, Nanjing, China
B.S. in Chemical Engineering, 1993

EXPERIENCE

The Pennsylvania State University, Aug. 1998-Aug. 2003
Biomolecular Transport Dynamics Laboratory
Department of Chemical Engineering
Graduate Research Assistant/ Teaching Assistant

Shanghai Research Center of Biotechnology, Chinese Academy of Sciences July 1996-July 1998
Principal Investigator and Research Associate

East China University of Science and Technology, Sep. 1993-July 1996
Department of Biochemical Engineering
Research Assistant

PUBLICATIONS

- Zhengyu Pang and John M. Tarbell, Flow and mass transport through the glycocalyx layer, (manuscript in preparation).
- Jeffry A. Florian, Jason R. Kosky, Kristy Ainslie, Zhengyu Pang, Randal O. Dull, and John M. Tarbell, heparan sulfate proteoglycan is a mechanosensor on endothelial cells, Circulation Research, (accepted).
- Zhengyu Pang and John M. Tarbell, In vitro study of Starling's hypothesis in cultured monolayer of bovine aortic endothelial cells, Journal of Vascular Research, (in press).
- Zhengyu Pang, Bo Guo, Yi Gong and Shengli Yang, Purification of recombinant CM11 protein from Escherchia coli., 97' symposium for Young Chinese Scholars on frontiers of biotechnology, 23, 1997, (in Chinese)
- Zhengyu Pang and Xingyan Wu, Affinity Chromatography of urokinase with a polystyrene-based medium, J. of East China University of Science and Technology, 22, 417-422, 1996, (in Chinese).

GRANT

Cloning, expression and purification of neurotoxin CM11, an 863 project from National (China) Science Foundation.